A Thesis

entitled

Numerical Modeling Methodology for the Strength Assessment of Deep Reinforced Concrete Members

by

Anish Sharma

Submitted to the Graduate Faculty as partial fulfillment of the requirements for the

Master of Science Degree in

Civil Engineering

_______________________________________

Dr. Serhan Guner, Committee Chair

_______________________________________

Dr. Douglas Nims, Committee Member

_______________________________________

Dr. Luis Mata, Committee Member

_______________________________________

Dr. Cyndee Gruden, Dean
College of Graduate Studies

The University of Toledo

May 2020

An Abstract of

Numerical Modeling Methodology for the Strength Assessment of Deep Reinforced Concrete Members

by

Anish Sharma

Submitted to the Graduate Faculty as partial fulfillment of the requirements for the Master of Science Degree in Civil Engineering

The University of Toledo
May 2020

Deep reinforced concrete members are typically encountered when designing bridge bents, pile-supported foundations, or transfer girders. These members should not be analyzed using the sectional method, which would underestimate their strengths. Additionally, the influence of the soil on the deep foundation members should be considered. AASHTO LRFD recommends the use of either a strut-and-tie or nonlinear finite element model for the analysis of deep members. Strut-and-tie method is iterative and assumes a linear-elastic stress field, which is still conservative. Nonlinear finite element analysis (NLFEA) has the capabilities to capture nonlinear strain distribution and soil nonlinearities. However, there is currently little guidance on how to conduct a numerical strength assessment of deep members using the NLFEA. The objective of this study is to use the NLFEA for the strength assessment of deep members while accounting for the deep beam action and soil influences.

For deep bridge bent beams, a strength assessment methodology is presented using the NLFEA while considering advanced concrete behavior such as tension stiffening,

compression softening, and dowel action. The proposed methodology is experimentally verified and applied for five existing deep bridge bent beams. In addition, the effectiveness of the proposed methodology is compared with the strut-and-tie and sectional analysis methods.

For the deep foundation cap beams, a methodology is presented for the holistic numerical strength assessment, including helical piles and considering the influence of soil. Important modeling considerations, such as soil-induced nonlinearities in the stress and strain fields, and soil-structure interactions are discussed, and experimental benchmarks are provided to assist practitioners in accurately modeling foundation systems.

Application of these methodologies can provide a realistic strength assessment of deep members, so that the rehabilitation funding can be directly efficiently.

# Acknowledgments

I would like to thank my advisor Dr. Serhan Guner for the invaluable opportunities, guidance, and encouragement provided, which were key in my academic and professional development. I would also like to thank the Ohio Department of Transportation (ODOT) of funding and supporting the first part of the research (Chapter 2). I am grateful to the ODOT technical liaisons, Mr. Matthew Blythe, P.E., and Ms. Andrea Parks, P.E., for their feedback and support, and to Ms. Michelle Lucas for managing the project and arranging monthly teleconferences. I am also grateful to the Deep Foundation Institute (DFI) for funding and supporting my studies as well as the second part of the research (Chapter 4).

Thank you to the thesis committee, Dr. Douglas Nims and Dr. Luis Mata, for their valuable suggestions and feedback. I am thankful to our research team for providing feedbacks and motivations. Special thanks to my colleague Rafael Salgado for his continuous assistance on my projects. I also acknowledge the Department of Civil and Environmental Engineering at The University of Toledo for providing the facilities required to conduct this research.

Thank you to my parents, and all my family and friends for their support and encouragement.

# Table of Contents

# List of Tables

## Chapter 2



## Chapter 3



## Chapter 4

# List of Figures

## Chapter 1



## Chapter 2

## Chapter 3



## Chapter 4

# 1. Introduction

Reinforced concrete deep members are widely encountered in buildings, bridges, and foundations. They commonly take the form of shear walls, bridge bent beams, foundation cap beams, and other configurations. Unlike shallow members, deep members exhibit a deep beam action that creates compression and tension paths (see Fig. 1). Consequently, plane sections do not remain plane in bending and the traditional design assumption of the sectional method does not apply (Collins and Mitchell 1991; Schlaich and Shafer 1991; Schlaich et al. 1987; Rogowsky and MacGregor 1986). In addition, the soil influences the behavior of deep foundation members, which is difficult to capture and thus usually neglected. The rapid increase in the number of deep reinforced concrete members has motivated the search for alternative methods that can achieve an improved understanding and accurate simulation of the behavior of these members.

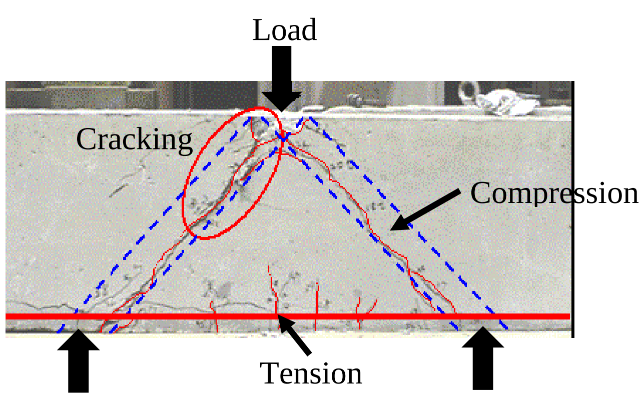


Fig. 1: Deep beam action.

AASHTO LRFD 2017 recommends the use of either a strut-and-tie or a nonlinear finite element method for the analysis and design of deep members. Strut-and-tie method (STM), which assumes a linear elastic stress field, is still conservative (Kim et al. 2011; Oh and Shin 2001; Kani 1967). Nonlinear finite element analysis (NLFEA), on the other hand, is shown to capture the nonlinear strain distributions (i.e. plane sections do not remain plane) and the effect of shear cracking (Pan et al. 2017; Demir et al. 2016).

Recent researches have demonstrated the advantages of the NLFEA for simulating the nonlinear behavior of deep members, as well as nonlinearities caused by the soil influence (George et al. 2017; Pan et al. 2017; Demir et al. 2016; Barbachyn et al. 2012; Zhou et al. 2011; Livneh et al. 2008). However, there is little guidance on how to use the NLFEA for determining the strength and safety of existing deep members, such as bridge bents and foundations.

In addition, discrete modeling approach is followed in the structural modeling of deep members, which typically neglects the soil influence with either a pinned or fixed support assumption (see Fig. 2a). On the other hand, geotechnical modeling neglects the deep foundation deformations with either pinned or fixed foundation assumption (see Fig. 2b). Therefore, the influence of the soil on the behavior of the deep foundation members is typically neglected.

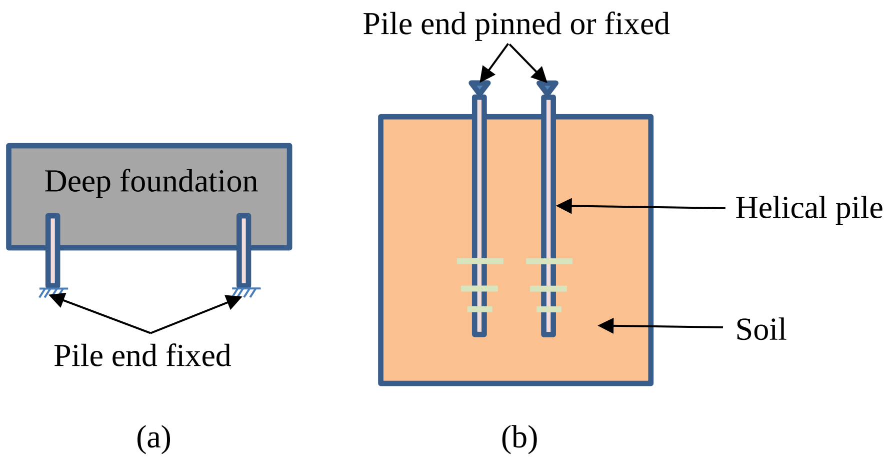


Fig. 2: Discrete modeling approaches in modeling of deep members considering (a) soil as fixed, and (b) foundation as pinned or fixed supported.

This study presents two methodologies for the use of NLFEA for the strength assessment of the deep bridge bents and deep foundation cap beams. For deep bridge bent beams, the methodology considers advanced concrete behavior such as tension stiffening, compression softening, and dowel action. The modeling approach is experimentally verified by investigating crack patterns, load-displacement response, failure modes, and governing critical members under near collapse conditions. The proposed methodology is employed on five existing bridges located in Ohio; the predicted capacities are compared with the traditional sectional and strut-and-tie method. For the deep foundation cap beams, another methodology is proposed for the holistic numerical modeling, including helical piles and accounting for the soil influence. The proposed modeling methodology is based on calibrating the material and interaction properties with the experimental benchmarks to capture the holistic response. These experimental benchmarks are discussed and presented to assist researchers in performing such calibrations. The discrete modeling approaches (i.e., considering soil as fixed support and foundation cap beam as fixed) are also investigated.

The proposed modeling methodologies aim to provide a strength assessment that is more accurate than the current analysis practice. This will result in more accurate assessment and ranking of overloaded deep members and save limited rehabilitation funds.

## 1.1 Scope and Objectives

To provide the guidance on how to use the NLFEA for strength assessment of existing deep members the following objectives were defined:

- Create and verify high-fidelity finite element models of reinforced concrete deep members,
- Develop a strength assessment methodology using NLFEA for the assessment of deep bridge bent beams,
- Verify the proposed NLFEA methodology with the experimental result of five deep bridge bents located in Ohio.
- Compare the effectiveness of the proposed NLFEA methodology with the sectional and strut-and-tie methods.
- Develop a holistic modeling methodology that allows accurate strength assessment of deep foundation cap beams, accounting for the soil interaction.
- Provide experimental benchmarks to assist practitioners in accurately creating the holistic foundation models.

## 1.2 Outline of the Document

This thesis is organized as follows. Chapter 2 presents an advanced numerical modeling methodology for strength evaluation of deep bridge bent caps. This chapter includes the journal paper's manuscript accepted in the American Concrete Institute (ACI) Special Publication. Chapter 3 includes the rating factors calculated for existing bridges using different analysis methods. Chapter 4 presents a holistic modeling methodology for helical pile and cap beam systems subjected to uplift loads. This chapter includes the manuscript submitted to the Engineering Structures journal. Chapter 5 summarizes the research results and global conclusions. Chapter 6 contains the references cited in this study.

# 2. Advanced Numerical Modeling Methodology for Strength Evaluation of Deep Bridge Bent Caps

This chapter includes the journal paper manuscript submitted to the American Concrete Institute by Anish Sharma and Dr. Serhan Guner. It is expected that there will be changes before the publication of the final paper. Please refer to the link https://www.utoledo.edu/engineering/faculty/serhan-guner/publications.html to download the final, published version of this paper.

## 2.1 Synopsis

Due to the increase in traffic and transported freight in the past decades, a significant number of in-service bridges have been subjected to loads above their original design capacities. Bridge structures typically incorporate deep concrete elements, such as cap beams or bent caps, with higher shear strengths than slender elements. However, many in-service bridges did not account for the deep beam effects in their original design due to the lack of suitable analysis methods at that time. Nonlinear finite element analysis (NLFEA) can provide a better assessment of the load capacity of deep bridge bent beams while accounting for the deep beam action. However, there is little guidance on how to conduct a numerical strength evaluation using the NLFEA. This study presents a nonlinear modeling methodology for the strength evaluation of deep bridge bents while considering advanced concrete behavior such as tension stiffening, compression softening, and dowel action. Five existing bridge bent beams are examined using the proposed methodology. The effectiveness and advantages of the proposed methodology are discussed by comparing the numerical results, including the load-displacement responses, load capacities, cracking patterns and failure modes, with the strut-and-tie and sectional analysis methods. Important modeling considerations are also discussed to assist practitioners in accurately evaluating deep bridge bents.

## 2.2 Introduction

Bridge structures typically incorporate deep reinforced concrete elements, such as bents or cap beams. Increases in traffic and transported freight over the past decade have increased the loading on the existing bridge bents, which requires accurate strength evaluation methods for making repair and strengthening decisions. Reinforced beams are typically subjected to a combination of axial, flexural and shear stresses. The commonly used bending theory (i.e., the sectional method) is based on the Bernoulli hypothesis, which assumes a linear distribution of strains through the section depth. However, bridge bent beams often have their shear span-to-depth ratios ($a/d$) less than 2.5, which qualifies them as deep beams. The behavior of deep beams must be treated separately because they do not exclusively exhibit a linear strain distribution (Collins and Mitchell 1991; Schlaich and Shafer 1991; Schlaich et al. 1987; Rogowsky and MacGregor 1986). Experimental work conducted on deep beams demonstrated that diagonal shear cracking is their main governing behavior (Scott et al. 2012; Kim et al. 2011; Oh and Shin 2001; Tan et al. 1997; Kani 1967; Clark 1951). The strut-and-tie-method (STM) is shown to represent the behavior of deep beams better than the sectional method (Baniya and Guner 2019; Kim et al. 2011; Oh and Shin 2001; Kani 1967). Various empirical formulations and analytical methods were proposed for evaluating the shear strength of deep beams based on the strut-and-tie approach (Gandomi et al. 2013; Scott et al. 2012; Guner and Vecchio 2010; Quintero-Febres et al. 2006; Hwang and Lee 2002; Oh and Shin 2001). However, these methods do not take into account the nonlinear material behavior and have limitations in predicting the post-peak softening behavior of deep beams, which is required for the prediction of displacement ductility. The complexity and uniqueness of bridge bents require a more advanced analysis approach such as nonlinear finite element analysis (NLFEA).

Current advances in computational capabilities of finite element modeling have been proven a versatile tool for studying the nonlinear pre- and post-peak behavior of structural members (Alsaeq 2013; Özcan et al. 2009). NLFEA by its nature is a global type of assessment, in which all structural parts interact. It has been shown to accurately model the nonlinear strain distributions and the effects of shear cracking on the stress and strain fields (Pan et al. 2017; Demir et al. 2016; Barbachyn et al. 2012). Recent researchers have demonstrated the possibilities and advantages of NLFEA for accurately simulating the nonlinear behavior of deep beams, including the effects of shear cracking and the nonlinearity of the strain distribution (Salgado and Guner 2018a, 2018b; Pan et al. 2017; Demir et al. 2016; Barbachyn et al. 2012; Niranjan and Patil 2012). However, there is little guidance on how to use the results from NLFEA for determining the strength and safety of existing bridge bents.

This study proposes a strength assessment methodology for bridge bent beams based on a pushover analysis performed using NLFEA. To achieve an accurate strength evaluation, NLFEA modeling of the deep bridge bents accounts for a number of advanced material behaviors including concrete confinement, compression softening, tension stiffening and softening, and reinforcement dowel action and buckling. The methodology uses a pushover analysis and a two-stage safety assessment procedure to determine a reserve or overload percentage for each bridge bent. The overall modeling process is presented through a case study, involving five existing bridge bents, to assist practitioners in accurately evaluating the strength of bridge bents. The effectiveness of the proposed methodology, as compared to the sectional and strut-and-tie methods, is also discussed.

## 2.3 Research Significance

Many in-service bridge bents did not account for deep beam effects in their original design. When analyzed using sectional methods, they are often found overloaded. NLFEA has the capabilities to capture the deep beam characteristics to more accurately predict the strength and ductility of deep bridge bents. However, there is a lack of methodologies on how to use the NLFEA, including the model development and the use of analysis results for the strength assessment of deep bridge bents. This study proposes a methodology using NLFEA and a two-stage safety assessment procedure to better interpret the holistic behavior and evaluate the strength of deep bridge bents.

## 2.4 Numerical Modeling and Safety Assessment Methodology

### 2.4.1 Finite element modeling

The proposed methodology uses a two-dimensional continuum-type finite element (FE) modeling approach. It can be applied using any FE modeling software on the condition that it is capable of simulating significant material behaviors including concrete confinement, compression softening, tension stiffening and softening, and reinforcement dowel action. The program VecTor2 (Wong et al. 2013) is used in this study, which employs a smeared, rotating crack model based on the Modified Compression Field Theory (MCFT) (Vecchio and Collins 1986) and the Distributed Stress Field Model (DSFM) (Vecchio 2000). The MCFT has been adopted by the AASHTO (2017) and CSA A23.3 (2014) codes. VecTor2 has been shown to provide an accurate simulation of the experimental behaviors in terms of strength, crack patterns, and the flow of principal stresses (Baniya et al. 2018; Senturk and Higgins 2010a). The graphical pre-processor, Formworks Plus (Wong et al. 2013), is used to create numerical models while the post-processor Augustus is used to visually examine the analysis results.

The concrete is modeled using 8-degree-of-freedom quadrilateral elements in geometrically uniform regions or 6-degree-of-freedom triangular elements in geometrically non-uniform regions as shown in Figs 1(a) and 1(b). The shear reinforcement is smeared into the concrete regions and the longitudinal reinforcement is discretely modeled as trusses through two-node elements with 2-degrees-of-freedom per node as shown in Fig. 1(c).

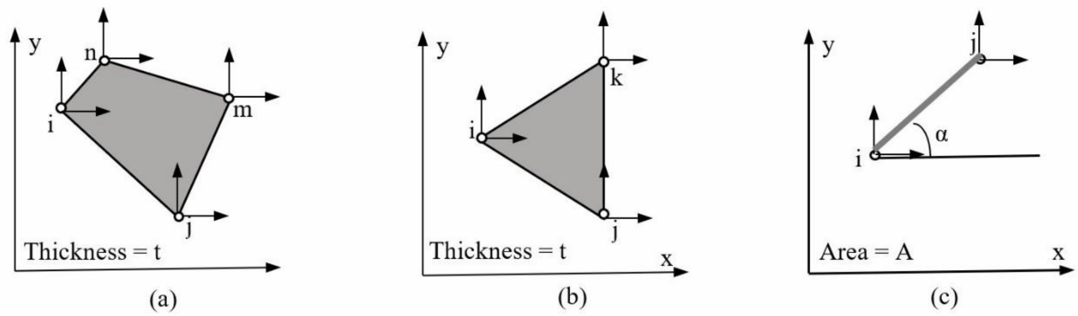


**Fig. 1 –** (a) Quadrilateral element for concrete, (b) triangular element for concrete, and (c) truss bar element for rebar

The NLFEA incorporates several advanced material behaviors specific to cracked reinforced concrete, as listed in Table 1. For deep bridge bents, four of these behaviors were found to be significant: concrete compression and tension softening, dowel action, and tension stiffening (Figure 2). Concrete compression softening is the reduction in the uniaxial compressive strength and stiffness due to transverse tensile cracking. The concrete tension softening, on the other hand, reduces the effectiveness of the concrete struts due to significant shear cracking that occurs when low amounts of stirrup reinforcement are present, which has been noticed in many bent beams. In addition, these low amounts of stirrups reduce the shear capacity such that the additional shear resistance due to dowel action becomes important. Finally, due to a lack of well-distributed layers of reinforcement in many older bent beams, they may exhibit flexural cracking, requiring the modeling of concrete tension stiffening effects.

**Table 1 –** Material models included in VecTor2.

| Material behavior | Model |
|---|---|
| Compression softening | Vecchio 1992-A |
| Tension stiffening | Modified Bentz 2003 |
| Tension softening | Linear |
| Rebar dowel action | Tassios (Crack slip) |
| Rebar buckling | Refined Dhakal-Maekawa |
| Crack width check | Max crack width of Agg/5 |
| Confinement strength | Kupfer/Richart |

Popovics (1973) and Modified Park-Kent (Bunni et al. 1982) models are employed for the pre- and post-peak response of the concrete, respectively. Even though the proposed methodology includes a static pushover analysis, the concrete model includes nonlinear hysteresis as shown in Figure 2(a) because some parts of the bridge bents will unload and reload, which is when the cracking of concrete and the yielding of reinforcement occurs. The stress between the concrete and reinforcement is transferred through the perfect bond. The steel reinforcement stress-strain response is composed of linear-elastic response, a yield plateau, and rupture in tension as shown in Fig. 2(b). Buckling of steel reinforcing is also taken into account (Akkaya et al. 2019).

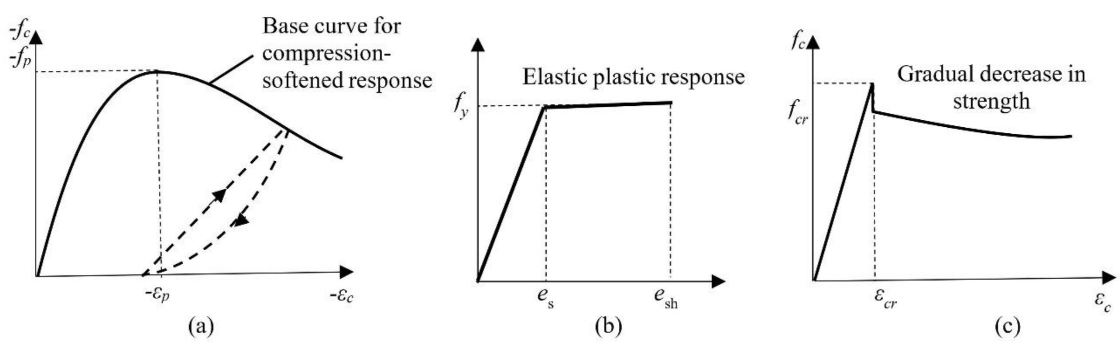


**Fig. 2 –** (a) Concrete, (b) reinforcing steel material constitutive models, (c) tension stiffening response

Multiple concrete regions are created to represent different smeared reinforcement conditions; Figure 3 shows an example. The reinforcement ratio ($\rho_t$) for each concrete region having a cross-sectional area of out-of-plane reinforcement ($A_b$), number of stirrups leg ($n$), spacing ($S_t$), and width of the cross-section ($W_c$), is calculated using Eqn. 1. The symmetry of the pier cap allows for modeling one-half of the beam, which reduces the analysis time. Rollers are defined at the axis of symmetry and pin supports are defined at the lowest ends of the pier (not shown in Fig. 3). Since no lateral load is considered, no significant stresses are developed in the column region and its effect can be neglected. Hence, the beam-column is considered monolithically jointed.

$$\rho_t = \frac{nA_b}{S_t\,W_c} \qquad (1)$$

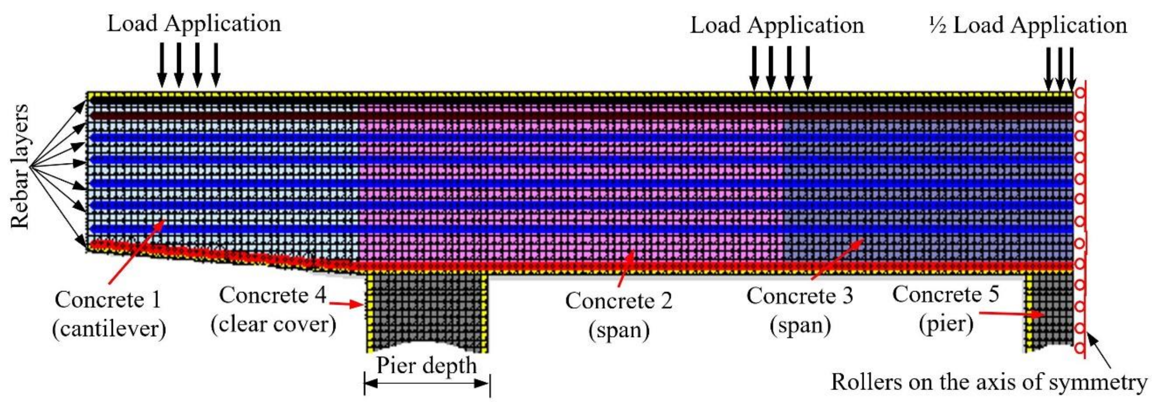


**Fig. 3 –** FE model developed for NLFEA

For the load application, the dead load is applied fully and then the live load is applied uniformly up to the failure of the beam. Maximum displacement is recorded. For bridge bent beams with a cantilever span, maximum displacement usually occurs at the tip of the cantilever span, whereas for bridge bent beams with no cantilever span, it occurs at the inner mid-span. A load-displacement curve can be generated so the load causing the failure of the bent beam can be determined.

### 2.4.2 Experimental verification of modeling approach

The accuracy of the proposed material modeling approach was verified with the results from experiments conducted on six full-scale in-service bridge bents by Senturk and Higgins at Oregon State University (Senturk and Higgins 2010b; Senturk 2008). These bridge bents resemble conventionally reinforced concrete deck girder (RCDG) bridges built in the 1950s. Five specimens had an overall height of 72 in. (1829 mm) and one specimen had an overall height of 48 in. (1219 mm). The width of the bent caps is 16 in. (406 mm). The support reaction and the location of the applied loads were the same for all specimens. The experimental results from two bridge bents were used to verify the cracking patterns and load-displacement responses determined from the proposed modeling approach. The details of the experimental setup and material properties were discussed by Senturk (2008). In short, the first specimen (originally referred to as D6.A2.G40#4.S) had a height of 72 in. (1829 mm), concrete strength of 3.52 ksi (24.4 MPa), reinforcing steel of yield strength 68.3 ksi (470 MPa), ultimate strength of 112.9 ksi (778 MPa), and #4 (13 mm) stirrups. For the second specimen (originally referred to as D4.A2.G40#4.S), the height of the beam was 48 in. (1219 mm) while the material properties were the same as for the first specimen.

The FE models of both specimens are shown in Fig. 4. One-half of the beam was modeled and rollers were provided on the axis of symmetry. Top and bottom reinforcement were modeled as truss elements and the shear reinforcement was smeared in the concrete. Material models listed in Table 1 were used. Fig. 4 shows the cracking conditions experimentally obtained (Senturk and Higgins 2010b; Senturk 2008) and numerically generated by the FE model. The shear cracking spanned from the support to the load application point, which indicated typical deep beam strut action. The FE model successfully captured the experimentally observed shear compression failure response as well as the strut action for both cases as shown in Fig. 4.

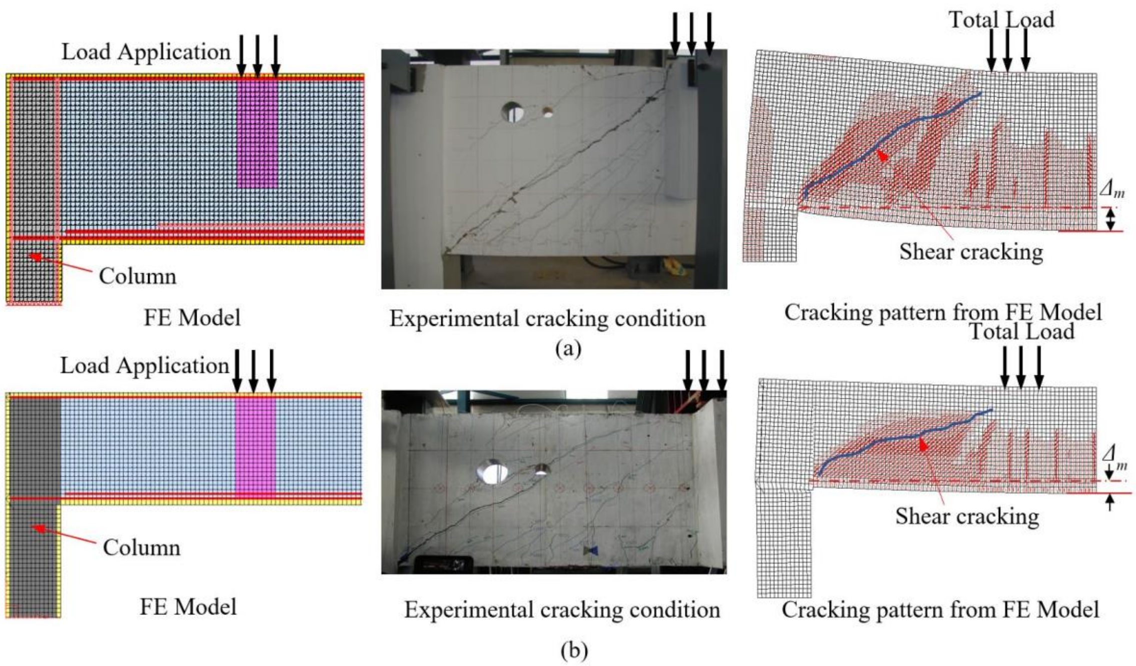


**Fig. 4** – FE model and cracking conditions for a) D6.A2.G40#4.S, and b) D4.A2.G40#4.S

Fig. 5 shows the total load and mid-span displacement ($\Delta_m$) response experimentally obtained (Senturk and Higgins 2010b; Senturk 2008) and numerically calculated by the FE model. The peak load, peak displacement and overall stiffness response of both beams were well captured by the FE model. The FE analysis to experimental ratios of the peak load capacity were 10% on average for the specimens.

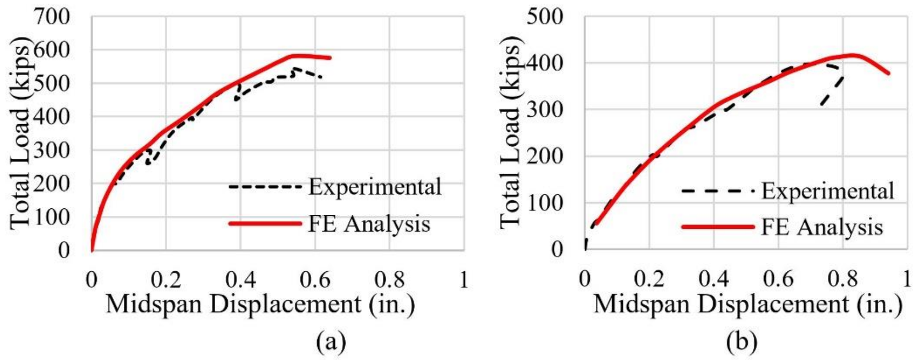


**Fig. 5 –** Load-displacement response for (a) D6.A2.G40#4.S, and b) D4.A2.G40#4.S; 1 in. = 25.4 mm and 1 kip = 4.45 kN

### 2.4.3 Two-stage safety assessment

The safety requirements for structural design require that the resistance of the structure exceed the demand of the total applied loads. The performance of a bridge depends on the uncertainties in loads and material resistances. NLFEA simulates a global response of the bridge bent beams. Thus, the NLFEA results require a safety assessment to be determined for the strength evaluation of bent beams. Many design codes, such as AASHTO (2017), consider the uncertainties in loads and material resistance by load and resistance factors. These safety factors are intended for the linear-elastic sectional analysis. If used in nonlinear analysis, they may change the stress distribution, failure mode, and overall response. Hence, a new two-stage safety assessment procedure is proposed in this study for nonlinear analysis as outlined in Fig. 6.

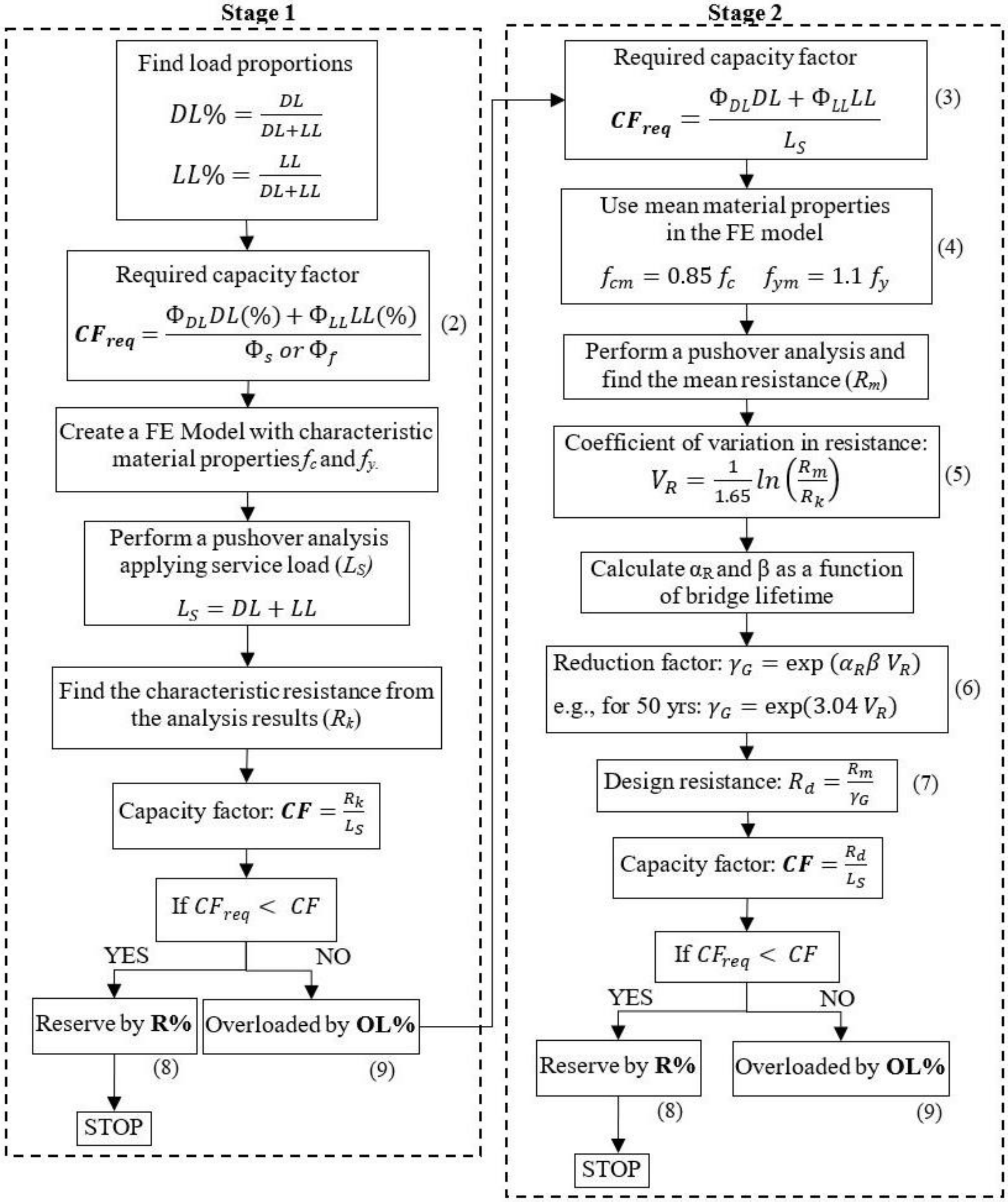


**Fig. 6 –** Proposed methodology for the two-stage safety assessment of bridge bents using NLFEA

As summarized in Fig. 6, the goal of the two-stage safety assessment is to find the required and actual capacity factors of the bridge beam. Stage 1 considers both the load and material resistance factors in the determination of the required capacity factor. This stage is simple to perform, requiring a single pushover analysis with characteristic (i.e., nominal) material properties. Stage 2 does not consider the material resistance factors when determining the required capacity factor; these factors are taken into consideration more precisely and probabilistically in the FE model. Compared to Stage 1, Stage 2 is more involved and requires two pushover analyses: one with the characteristic material properties and another with the mean material properties. Stage 2 assessment is only required if the bridge is found overloaded in Stage 1.

In Stage 1, the proportion of the dead load (DL) and live load (LL) with respect to the total load is determined first. Then, the load combination from the AASHTO (2017) specifications is followed to determine the factored load proportions to be used in Eqn. 2 (shown in Fig. 6). Any other code specifications may be used depending on the location of the structure. The factored load is divided by the shear reduction factor (ΦS) or flexural reduction factor (Φf) to determine the required capacity factor (CFreq) for the bridge bent beam as defined in Eqn. 2. The choice of material reduction factor depends on the mode of failure of the structure (ACI 318-19). The bridge bent beam is modeled in an FE software with characteristic material properties. The pushover analysis is then performed applying the service load (LS), where total DL is applied initially and LL is applied uniformly until failure of the beam. The resistance (Rk in Fig. 6) is determined from the load-displacement (i.e., pushover) curve. The actual capacity factor (CF), is determined as the ratio between

Rk and the service load (LS). If it is higher than the required capacity factor, the bridge bent is classified as safe. Otherwise, it is overloaded and a Stage 2 assessment should be made.

In Stage 2, the required capacity factor is determined as the ratio between the factored loads and LS as defined in Eqn. 3 (shown in Fig. 6). A comparison of Eqns. 2 and 3 shows that the material resistance factors are not used while determining the required capacity factor in Stage 2. This stage requires another NLFEA using mean material properties. For this, the mean yield strength of steel (fym) and the mean compression strength of concrete (fcm) are estimated from the characteristic concrete compressive strength (fc) and steel yield strength (fy) as defined in Eqn. 4 (shown in Fig. 6) (Cervenka 2008). A second pushover analysis is then performed to find the mean resistance (Rm) of the beam. The coefficient of variation of the resistance (VR) is then calculated using Eqn. 5, where Rk and Rm are the resistances of the element using its characteristic and mean properties of materials, respectively. A reduction factor ($\gamma$G) is probabilistically obtained using Eqn. 6, which is based on the sensitivity factor for the resistance reliability ($\alpha$R) and the reliability index ($\beta$), factors that depend on the service life of the bridge as shown in Fig. 7(a). For a service life of 50 years, recommended values for the ultimate limit states are 0.8 and 3.8, respectively (Cervenka 2008). For a service life of 75 years, $\alpha$R and $\beta$ are 0.8 and 3.2, respectively. Similarly, AASHTO (2017) recommends $\beta$ of 3.5 for bridges. The sensitivity of $\gamma$G with respect to service life is shown in Fig. 7(b), which indicates differences below 5% for 50 or 75 years of structural service life. In this study, the reduction factor was calculated considering a service life of 50 years. The design resistance (Rd) is then obtained using the mean resistance (Rm) and γG as defined in Eqn. 7. The CF is determined as the ratio between Rd and Ls. If CF is more than CFreq, the bridge bent beam is considered safe; otherwise, it is considered overloaded.

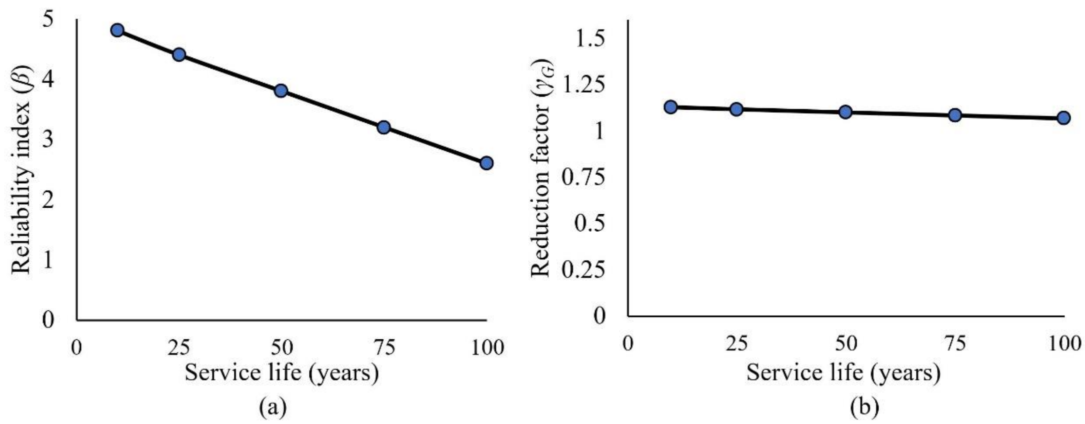


**Fig. 7 –** (a) Reliability index versus service life, and (b) Reduction factor versus service life

The reserve capacity (*R%*) and the overload capacity (*OL%*) of the bridge bent beams can be determined in any stage using Equations 8 and 9, respectively.

$$R\% = \left(\frac{CF}{CF_{req}} - 1\right) * 100 \qquad (8)$$

$$OL\% = \left(1 - \frac{CF}{CF_{req}}\right) * 100 \qquad (9)$$

## 2.5 Application of the Proposed Methodology

To demonstrate the application of the proposed methodology, five bent beams (four with and one without cantilever spans) of existing bridges were modeled as shown in Table 2. The concrete characteristic compressive strengths for these beams ranged from 4 ksi (27.6 MPa) to 4.5 ksi (31 MPa); the number of piers ranged from three to seven; beam depths (*d*) ranged from 36 inches (915 mm) to 48 inches (1220 mm); and shear span-to-depth ratios (*a/d*) ranged from 0.10 to 3.03; hence, most spans qualify as deep beams. The steel reinforcement characteristic yield stress was 55 ksi (378 MPa). As an example, the configuration and NLFEA model of Bridge 1 is shown in Figs 8 and 9, respectively.

**Table 2 –** Bridge bents details; 1 ft = 304.8 mm and 1 in.$^2$ = 645.2 mm$^2$

| Bridge | $w$ (ft) | $d$ (ft) | $t$ (ft) | a/d Min | a/d Max | $A_y$ (bottom) (in.$^2$) | $A_y$ (top) (in.$^2$) |
|---|---|---|---|---|---|---|---|
| Bridge 1 | 44 | 4 | 3 | 1.40 | 1.89 | 7.00 | 13.95 |
| Bridge 2 | 51.17 | 3.5 | 3.5 | 0.10 | 1.91 | 8.00 | 9.46 |
| Bridge 3 | 64.67 | 3.5 | 3 | 0.19 | 2.80 | 8.00 | 8.00 |
| Bridge 4 | 53.33 | 4 | 3 | 0.50 | 1.51 | 9.00 | 8.00 |
| Bridge 5 | 87 | 3 | 3 | 0.14 | 3.03 | 7.90 | 7.90 |

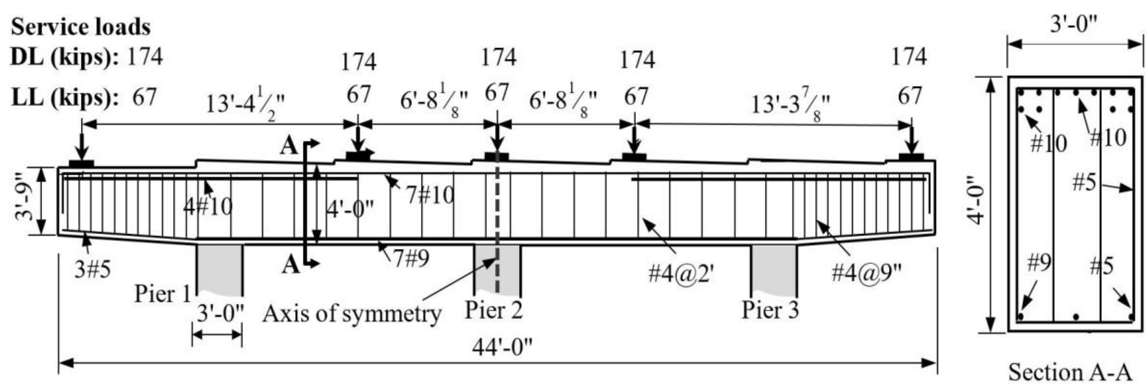


**Fig. 8 –** Bridge 1 bent elevation and cross-section; 1 in. = 25.4 mm and 1 kip = 4.45 kN

The symmetry of the beams allowed for a one-half model, which significantly reduced the modeling effort and computation time. The lowermost ends of the columns were pinned while rollers were used on the axis of symmetry. Regions with different shear reinforcement are represented by different colors in Fig. 9. The shear reinforcement in each region was calculated using Eqn. 1. A convergence test was performed for mesh size ranging from 20 to 100 mm. An FE mesh size of 50 x 50 mm satisfactorily balanced accuracy and computing time and hence, was used in modeling. Pushover analyses were performed with the total dead load applied initially; the live load was then increased in fixed increments of 10% until failure. The load-displacement responses were generated, and the strength evaluation was performed based on the proposed two-stage safety assessment procedure.

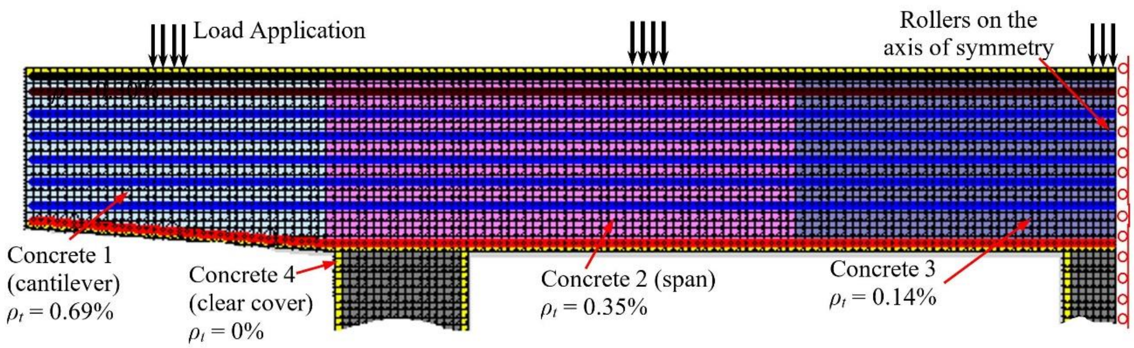


**Fig. 9 –** FE model developed for Bridge 1

The sample beam shown in Figs 8 and 9 was originally designed using the Strength I ultimate load combination of *1.25DL + 1.75LL* and the shear reduction factor ($\Phi_S$) of 0.75 (ACI 318-19). Based on the load and material resistance factors, $CF_{req}$ was determined to be 1.90 from Stage 1 assessment. An FE model was created with the characteristic material properties. The factored dead load of 217.5 kips was fully applied and then the live load was gradually applied until failure of the beam. From a single pushover analysis performed with characteristic material properties, $R_k$ was determined to be 1456 kips (6480 kN). The *CF* of the bridge bent was determined to be 2.41, following the methodology discussed above {i.e., 1456 / [(174+67) x 2.5]}. The capacity factor was found to be higher than the required, and the reserve capacity was calculated using Eqn. 8 to be 27% as shown in Fig. 10(a). Since the bridge was found to be safe, there was no need to perform Stage 2 assessment. However, for demonstrative purposes, Stage 2 assessment was undertaken as follows.

The required capacity factor in Stage 2 is determined as the ratio of the factored load to the service load, which was found to be 1.42 for the analyzed beam. The required capacity factor only considers uncertainties in load (i.e., load factors), while the FE model captures the material uncertainties. An additional pushover analysis was performed with the mean material properties as shown in Fig. 10(b). The mean resistance was determined to be 1554 kips (6915 kN). As discussed above, the coefficient of variation and reduction factors were determined for 50 years of service life. The design resistance of the cap beam was then calculated to be 1665 kips (7410 kN), which corresponds to a *CF* of 2.53. Consequently, the cap beam was found to be safe, as expected, with a 78% reserve capacity.

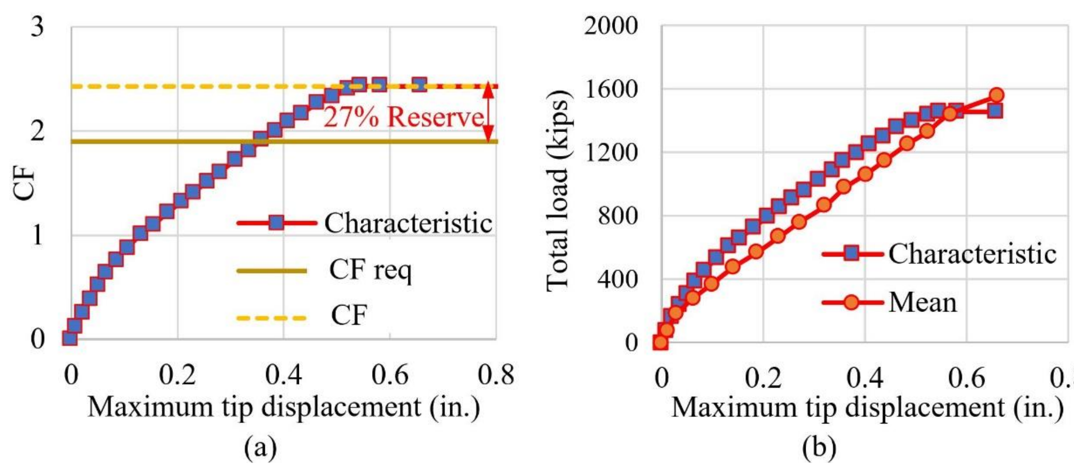


**Fig. 10 –** Response of Bridge 1 for (a) Stage 1 and (b) Stage 2; 1 in. = 25.4 mm and 1 kip = 4.45 kN

The methodology was applied, in a similar manner, to the remaining four bridges. The models for each bent beam are shown in Fig. 11(a). Shear and flexural crack patterns at the failure conditions are presented in Fig. 11(b). Initial cracks typically occurred at the mid-span bottom faces of interior spans as flexural cracks. With the increase in loading, more cracks formed, and the widths of the existing cracks increased. Diagonal compression struts formed in the beams, which represent the deep beam strut action (i.e., shear cracks spanned from the point loads to the column supports). Vertical flexural cracks formed above the column regions, with yielding of the top rebar at those locations. The conditions of the top and bottom reinforcement of the beam are also shown in Fig. 11(c). From the cracking pattern, it is clear that the bridge bents are shear critical at the cantilever spans and inner spans near the columns. The yielding of the top and bottom flexural reinforcement of the bridge bent at the beam-column interface caused crushing of the concrete, resulting in a shear-flexural failure mode.

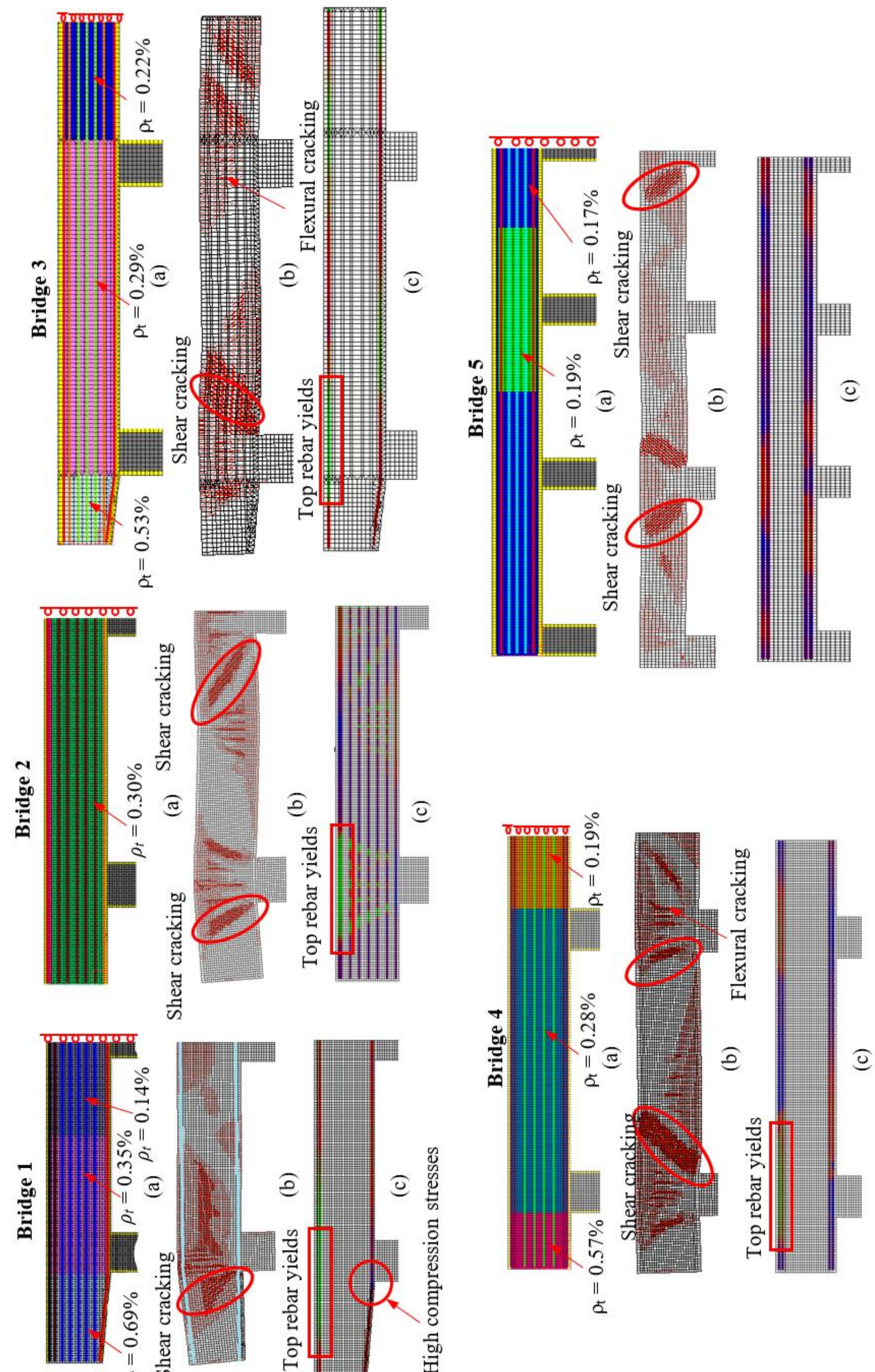

Bridge 1
$\rho_t = 0.69\%$
$\rho_t = 0.35\%$
$\rho_t = 0.14\%$
(a)
Shear cracking
(b)
Top rebar yields
High compression stresses
(c)
Bridge 2
$\rho_t = 0.30\%$
(a)
Shear cracking
Shear cracking
(b)
Top rebar yields
(c)
Bridge 3
$\rho_t = 0.53\%$
$\rho_t = 0.29\%$
$\rho_t = 0.22\%$
(a)
Shear cracking
Flexural cracking
(b)
Top rebar yields
(c)
Bridge 4
$\rho_t = 0.57\%$
$\rho_t = 0.28\%$
$\rho_t = 0.19\%$
(a)
Shear cracking
Flexural cracking
(b)
Top rebar yields
(c)
Bridge 5
$\rho_t = 0.19\%$
$\rho_t = 0.17\%$
(a)
Shear cracking
Shear cracking
(b)
(c)

**Fig. 11 –** (a) Finite element model developed, (b) Crack pattern (10 times actual deflection) , and (c) Rebar stresses at failure

The combined results for all five bridges indicate that all of the bridges are safe in both stage assessments under the existing loading condition. The material resistance factors used in Stage 1 (see Eqns. 2 and 3 in Fig. 6) were typically conservative and provided a higher required capacity factor as shown in Table 3. On the other hand, Stage 2 does not consider material resistance factors to determine the required capacity factor, which resulted in a lower required capacity factor as shown in Table 3. Thus, Stage 2 provided a less-conservative assessment approach and, consequently, higher reserve capacities for all of the bridge bents analyzed in this study.

**Table 3 –** Safety evaluation results of deep bridge bents

| Bridge Name | Capacity (kips) | Stage 1 | | | Stage 2 | | |
|---|---|---|---|---|---|---|---|
| | | $CF_{req}$ | $CF$ | Reserve | $CF_{req}$ | $CF$ | Reserve |
| Bridge 1 | 1456 | 1.90 | 2.41 | 27% | 1.42 | 2.53 | 78% |
| Bridge 2 | 2976 | 1.89 | 4.12 | 118% | 1.42 | 4.21 | 196% |
| Bridge 3 | 2565 | 1.89 | 3.18 | 68% | 1.41 | 3.42 | 142% |
| Bridge 4 | 2340 | 1.94 | 2.97 | 53% | 1.46 | 2.87 | 97% |
| Bridge 5 | 3885 | 1.91 | 2.36 | 24% | 1.43 | 2.54 | 77% |

NOTE: 1 kip = 4.45 kN

## 2.6 Comparisons with Sectional and Strut-And-Tie Methods

Bridge pier caps are commonly designed using the sectional method, even though this method cannot account for the deep beam action. To demonstrate the capacities obtained, the five bent beams analyzed with the NLFEA were also analyzed using the sectional method. The moment and shear capacities were determined at the critical sections based on the AASHTO LRFD (2017) code. The sectional analysis results indicated that all beams were significantly overloaded in shear. The proposed NLFEA methodology, on the other hand, found significant reserve shear capacities for the same beams by predicting 2.5-times the shear capacity, on average, compared to that obtained from the sectional method as shown in Fig. 12(a).

The same bent beams were also analyzed using the strut-and-tie-method (STM) (Scott et al. 2012), using the computer program STM-CAP (Baniya et al. 2018), which is a Visual Basic Advanced (VBA)-based graphical computer program developed specifically for pier caps. Fig. 12(b) shows the ratio between the capacities calculated by the NLFEA and the STM. While STM provided larger capacities than the sectional method, the predicted capacities were still much smaller than the proposed NLFEA methodology. The proposed NLFEA methodology predicted 1.5-times the shear capacity, on average, compared to that obtained from STM as shown in Fig. 12(b).

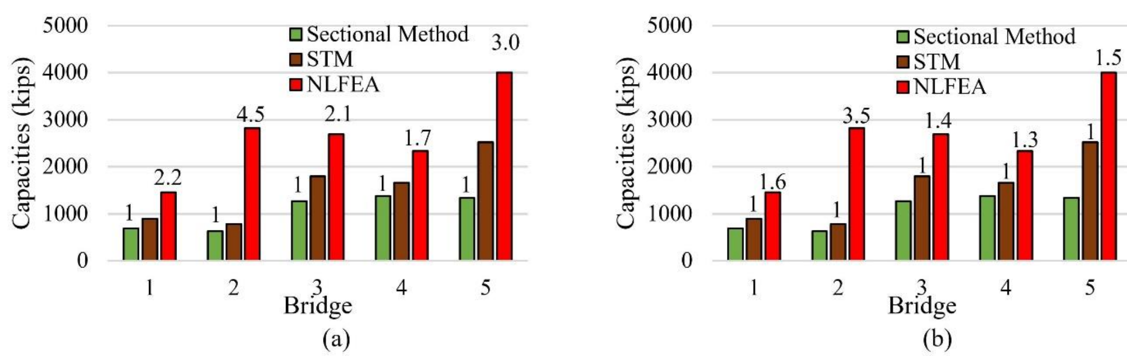


**Fig. 12 –** Comparison of shear capacities from NLFEA with (a) Sectional method and (b) STM; 1 kip = 4.45 kN

Fig. 13 shows the capacities and the load-displacement responses obtained from all three methods. For the purpose of comparison, the capacities are normalized to the capacities obtained from the sectional method. In most cases, the pushover responses exhibit an initial linear portion with high stiffnesses followed by nonlinear responses due to concrete cracking and steel yielding. When comparing the calculated capacities of the sectional and STM methods with the pushover curve and failure modes of the NLFEA, results in Fig. 13 show that the sectional method predicts the capacities shortly after the linear-elastic region, while the STM predictions are based on either the first yielding of reinforcement or first local crushing of the concrete. Both methods neglect the strain hardening behavior of reinforcement and the re-distribution of stresses due to concrete cracking and reinforcement yielding.

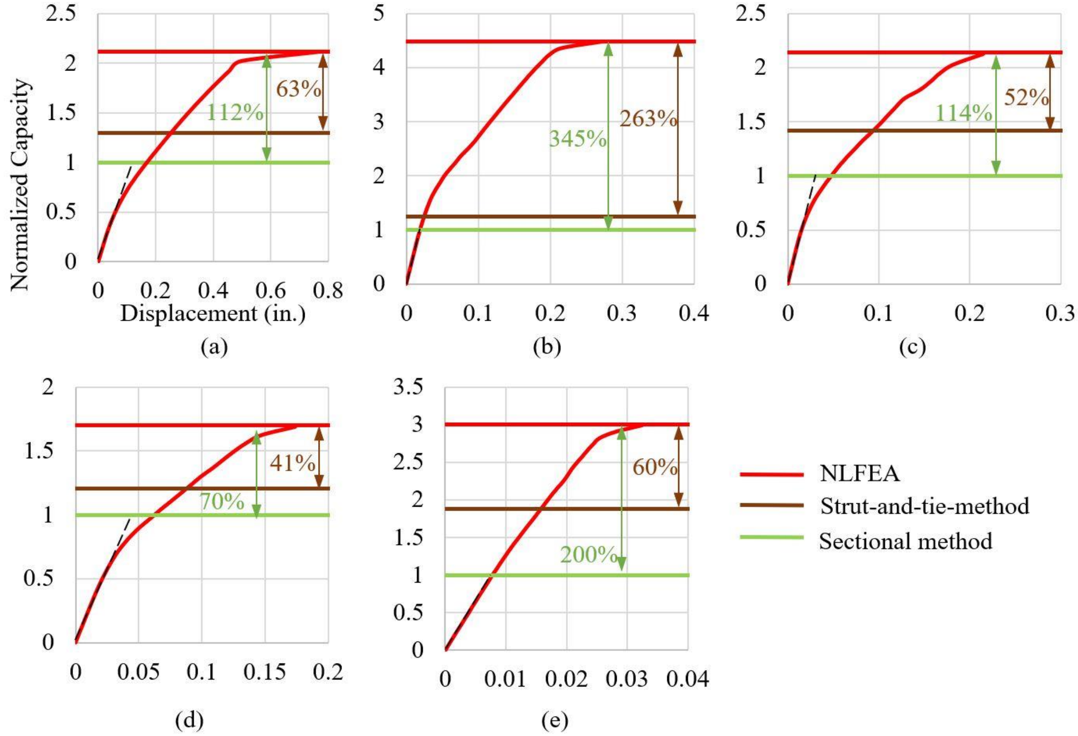


**Fig. 13 –** Load displacement response of (a) Bridge 1, (b) Bridge 2, (c) Bridge 3, (d) Bridge 4, and e) Bridge 5; 1 in. = 25.4 mm

## 2.7 Simulation of Load Redistribution

In all of the beams examined, it was found that the failure did not occur at the first yield of reinforcement or first crushing of concrete. There was a significant redistribution of the stresses, which subsequently provided higher load capacities. Bridge 2, for example, showed significant load re-distribution, which resulted in higher differences in the load capacity as compared to the sectional method and STM, as seen in Fig. 13(b). The crack patterns and the rebar stresses in the top and bottom reinforcement bars are shown in Fig. 14 for the initial, first major damage and failure conditions. Cracks initially formed at mid-span as shown in Fig. 14(a). Diagonal cracks did not form during the elastic part of the response. The sectional method considered the failure at the critical sections during this stage, which was overly conservative. However, in the NLFEA, the stresses in the main longitudinal reinforcement kept increasing and penetrating further into the beam, which prevented any localized failure. As a result, widespread cracks were formed. The capacity indicated by the strut-and-tie-method corresponds to Fig. 14(b), where the first rebar yielded. After the top reinforcing bar yielded, 2-times higher load could be supported by the beam until the shearing of the concrete as shown in Fig. 14(c). The failure occurred from yielding of the reinforcement and shearing of the concrete along the beam length. Consequently, the proposed NLFEA methodology was useful when investigating the load redistribution and the sequence of nonlinear occurrences.

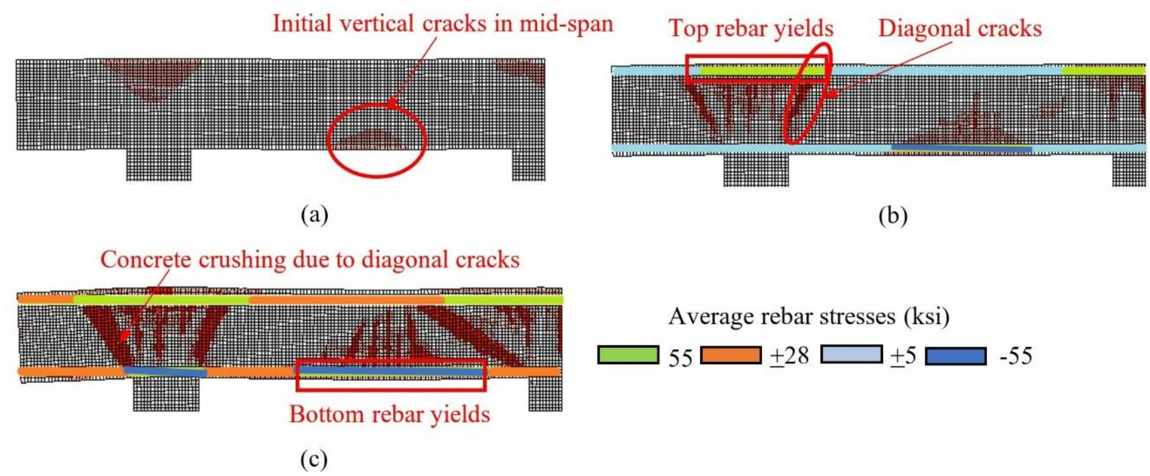


**Fig. 14 –** (a) First cracking, (b) First rebar yielding, and (c) Failure crack patterns and rebar stresses obtained from the NLFEA for Bridge 2; 1 ksi = 6.9 MPa

## 2.8 Summary and Conclusions

A nonlinear finite element analysis (NLFEA) methodology is proposed for the strength evaluation of deep bridge bents. The assessment employs a two-stage safety assessment procedure and considers advanced concrete behaviors such as tension stiffening, compression softening, and dowel action. The application of the proposed methodology is presented by examining five existing bridge bents. The effectiveness of the proposed methodology is discussed and a comparison with sectional and strut-and-tie methods is made. The results of this study support the following conclusions.

1. Most bridge bents are deep beams with nonlinear strain distributions. Analysis methods capable of representing the deep beam action are required to obtain accurate results.
2. The proposed NLFEA methodology was shown to simulate the nonlinear stress/strain distributions, the sequence of nonlinear occurrences and redistribution

of forces after concrete cracking and rebar yielding, and the governing failure mechanisms.

3. The proposed two-stage safety assessment procedure simplified the strength assessment process by employing the concept of a capacity factor based on the load and material resistance factors. If the bridge is found overloaded in Stage 1, a more in-depth probabilistic assessment of Stage 2 is required. Stage 2 assessment was shown to predict higher reserve shear capacities than Stage 1 assessment; on average, the difference in capacity was 2-times for the bridges examined in this study.
4. The conventional sectional methods cannot capture the nonlinear strain distribution and thus are not suitable for the analysis of deep beams. The proposed NLFEA methodology predicted 2.5-times the shear capacities, on average, compared to the sectional analyses (performed for demonstrative purposes).
5. The strut-and-tie method was found to provide a strength prediction corresponding to the first yielding of the reinforcement or first crushing on the concrete, without accounting for any force redistribution. The proposed NLFEA methodology predicted 1.5-times the shear capacities, on average, compared to the strut-and-tie analyses.
6. The proposed NLFEA methodology was useful when investigating the load redistribution and the sequence of nonlinear occurrences. Redistribution of the stresses with the subsequent development of nonlinear occurrences was found to provide 2-times the load capacity for one of the bridge bents investigated.

7. There is limited public funding for the rehabilitation and strengthening of the existing bridges. NLFEA that considers the required material models offers the potential to correctly identify and rank overloaded bridges so that available funds can be directed to the most critical bridges.

## 2.9 Acknowledgment

The authors would like to thank the Ohio Department of Transportation for providing the structural design drawings and PhD candidate Rafael A. Salgado and MS candidates Pappu Baniya, Sálvio A. Almeida Jr., and Sundar Chiluwal, at the University of Toledo, for their feedback and support in this study.

## 2.10 Notations

$a/d$ Shear span-to-depth ratio

$\alpha_R$ Sensitivity factor for the resistance reliability

$A_b$ Cross-sectional area of out-of-plane reinforcement

$A_y$ Cross-sectional area of main reinforcement

$\beta$ Reliability index

$CF$ Capacity factor

$CF_{req}$ Required capacity factor

$\Delta_m$ Mid-span displacement in the beam

$d$ Depth of beam

$f_c$ Concrete characteristic uniaxial compressive strength

$f_{cm}$ Concrete mean uniaxial compressive strength

$f_s$ Reinforcement rupture strength

$f_y$ Reinforcement characteristic yield strength

$f_{ym}$ Reinforcement mean yield strength

$L_d$ Factored loads

$L_S$ Unfactored (service) loads

$\Phi_f$ Flexural-behavior reduction factor

$\Phi_S$ Shear-behavior reduction factor

$\rho_t$ Reinforcement ratio

$R_d$ Design resistance

$R_k$ Resistance obtained using characteristic material properties

$R_m$ Resistance obtained using mean material properties

$\gamma_G$ Reduction factor

$S_t$ Spacing of stirrups

$V_R$ Coefficient of variation of resistance

$w$ Width of beam (average)

$W_c$ Width of beam cross-section

# 3. Load rating of existing bridges using STM and NLFEA.

The increase in traffic and transport freight over the past decade has significantly increased the live loads on existing bridge structures. The funds for maintaining and strengthening these bridges are limited; hence, accurate analysis methods are required for their load rating. It is generally observed that the capacities of bridges are evaluated using the sectional method and rated as per the AASHTO bridge evaluation manual in terms of rating factor (RF). However, deep concrete members in bridges possess additional shear strengths due to the formation of the strut action, which cannot be captured by the conventional sectional method. To overcome this limitation, a methodology was proposed in Chapter 2, which provides a well-defined framework using nonlinear finite element analysis for the strength evaluation of deep bridge bent beams. The proposed methodology quantifies the strength limits for bridge bent beams in terms of their capacity factor (CF). The existing bridge load rating procedure in AASHTO LRFD standard employs RF for the load rating of bridges. This chapter presents an additional method to determine RF for the bridges using more accurate analysis methods recommended by AASHTO (i.e. strut-and-tie method and nonlinear finite element analysis). Five existing bridge bent beams are evaluated and compared in terms of RF, which reveals 2.5 times higher RF from STM and

4 times higher RF from NLFEA, reducing the number of overloaded bridges for strengthening.

## 3.1 Introduction

Most bent beams in existing bridges were designed using older standards and lighter loads. The increase in the live load due to heavier traffic, additional lanes, and transported freight has now centered the emphasis of bridge engineering on maintenance and strengthening of the existing bridges. The funds for maintaining and strengthening these bridges are limited; hence, accurate analysis methods capable of representing the deep beam action is required to correctly identify and rank the overloaded bridge bent beams while performing a load rating.

In civil engineering practice, the sectional method is the most popular method and is dominantly used for analyzing and load rating existing bridges. Although it only applies to slender beams, it is commonly used for deep beams with the end result of providing overly conservative results. AASHTO LFRD (2017) requires the use of either a strut-and-tie or a nonlinear finite element analysis for deep beams. The strut-and-tie-method (STM) is shown to represent the behavior of deep beams more accurately than the sectional method (Baniya and Guner 2019; Kani 1967). In addition, recent research has demonstrated the possibility and advantages of nonlinear finite element analysis (NLFEA) for accurately simulating the behavior of deep beams, including the effects of shear cracking and the nonlinear strain distributions (Sharma and Guner 2019; Demir et al. 2016).

This chapter presents a method for using the STM and NLFEA for load rating of existing bridge bents and obtaining their safe live load carrying capacity in terms of rating factors (RFs). The method is presented for five existing bridges located in Ohio. Predicted RFs are compared with the RF obtained from the conventional sectional capacity.

## 3.2 Bridge load rating

Bridge load rating is a procedure to evaluate the safe live load carrying capacity of an existing bridge. For load rating of a bridge, the rating factor (RF) is used as a scaling factor. The RF provides an estimate of the relationship between the reserve live load carrying capacity of a bridge and the live load demand. An RF value greater than 1.0 indicates a reserved live load carrying capacity while a value less than 1.0 indicates an overload. The RF used within the current AASHTO manual for bridge evaluation is based on a load and resistance factor rating method, given as follows:

$$RF = \frac{\Phi C - \Upsilon_{DC} DC - \Upsilon_{DW} DW \pm \Upsilon_{p} P}{\Upsilon_{LL} LL(1+IM)} \quad (1)$$

Since the behavior of deep beam bridge bents is typically governed by shear failures, this study will focus on the shear capacity calculations. The same procedure can be applied to the flexural capacities as well. The shear capacity (C) is determined from three different methods in this study; namely, the sectional method, STM, and NLFEA, which will be discussed below.

## 3.3 Determination of rating factors

In this section, rating factors are determined for five existing bridges using the capacity determined from the sectional method, STM, and NLFEA. The details of the geometric and material properties for these bridges are discussed elsewhere (Baniya et al. 2018).

### 3.3.1 Sectional method

The sectional method requires checking the shear (or moment) capacities at critical sections based on the "plane-sections-remain-plane" hypothesis, which is not valid for deep beams. Although the sectional method should not be used for deep beams, it is used in this study for comparison purposes. Since most deep beams fail in shear, the most critical section is determined from the shear force diagram of the bridge. The sectional shear capacity (C) is determined using the applicable concrete design code, AASHTO LRFD in this case. The dead load (DL) and live load (LL) acting on the critical section are considered with an impact factor (IM) of 33% applied to the live load to predict the rating factor (RF), as shown in Equation 2.

$$RF = \frac{\Phi C - \Upsilon_{DL} DL}{\Upsilon_{LL} LL * (1 + IM)} \qquad (2)$$

The strength I limit state is considered where the dead load factor $\Upsilon_{DL}$ is 1.25 and the live load factor $\Upsilon_{LL}$ is 1.75. The detailed calculation results obtained from Equation 2 are shown in Table 1.

**Table 1:** Calculation of rating factor (RF) from the sectional method.

| | ***C*** **(kips)** | ***DL*** **(kips)** | ***LL*** **(kips)** | ***RF*** |
|---|---|---|---|---|
| **Bridge 1** | 545 | 172 | 66 | 1.26 |
| **Bridge 2** | 550 | 120 | 43 | 2.66 |
| **Bridge 3** | 470 | 151 | 53 | 1.32 |
| **Bridge 4** | 425 | 121 | 60 | 1.20 |
| **Bridge 5** | 550 | 114 | 46 | 2.54 |
| | | | Average: | 1.80 |

The rating factors predicted are all larger than 1.0; hence, all bridges are structurally safe under the applied live loads, with bridges 1, 3, and 4 exhibiting the least potential of carrying extra live load. It should be noted that these bridge bents are deep and possess additional shear capacity due to the formation of the strut action, which is not considered in the sectional method.

### 3.3.2 Strut-and-tie method

The strut-and-tie method (STM) uses a truss model where the stress field in the structural concrete is equivalent to a hypothetical simple uniaxial truss structure which defines the load paths. STM is conceptually a simple design methodology suitable for deep beams. However, its implementation is complicated, requiring a graphical solution procedure. In this study, the computer program STM-CAP (Baniya et al. 2018) is used.

STM-CAP determines the failure load ($P_f$) of the weakest member using an automatically generated STM model. RF is determined based on the live load, which causes the shear failure of a member in STM. The factored dead load (*1.25DL*) is subtracted from $P_f$, which yields the total live load carrying capacity of the model. The ratio of this total live load carrying capacity to the applied live load (factored by *IM*) gives the RF for the STM model, as shown in Equation 3. Using this equation and the failure load $P_f$ from the STM model, the RFs are calculated for each bridge bent as shown in Table 2.

$$RF = \frac{P_f - 1.25DL}{LL * (1 + IM)} \qquad (3)$$

**Table 2:** Calculation of rating factor (RF) from STM.

| | ***1.25DL*** **(kips)** | ***LL*** **(kips)** | **$P_f$ (kips)** | ***RF*** |
|---|---|---|---|---|
| **Bridge 1** | 215 | 66 | 475 | 2.95 |
| **Bridge 2** | 150 | 43 | 520 | 6.55 |
| **Bridge 3** | 189 | 53 | 515 | 4.61 |
| **Bridge 4** | 151 | 60 | 460 | 3.87 |
| **Bridge 5** | 142 | 46 | 465 | 5.27 |
| | | | Average: | 4.65 |

### 3.3.3 Nonlinear finite element analysis

Nonlinear finite element analysis (NLFEA) is an advanced numerical analysis method that can be used to predict the capacities of deep bridge bents. When applied considering advanced material models, such as tension stiffening, compression softening, and dowel action, it offers significant potential for accurate simulation of the behavior of deep bridge bents.

NLFEA predicts the system-level response and the use of material resistance factors in the material models can artificially influence the response and failure mode of the bridge bent beam. Thus, NLFEA models without material resistance factors are analyzed to obtain the system level failure loads ($P_f$), which are then multiplied by the governing resistance factor ($\Phi$) – shear in this case – to obtain the capacity of the entire beam. The RFs are determined by employing the total factored dead load ($DL_t$), the total live load ($LL_t$) and the impact factor ($IM$), as per Equation 4. The detailed calculation results are shown in Table 4.

$$RF = \frac{\Phi P_f - 1.25DL}{LL * (1 + IM)} \qquad (4)$$

**Table 3:** Calculation of rating factor (RF) from NLFEA.

| | $\boldsymbol{1.25DL_t}$ (kips) | $\boldsymbol{LL_t}$ (kips) | $\boldsymbol{P_f}$ (kips) | $\boldsymbol{\Phi P_f}$ (kips) | ***RF*** |
|---|---|---|---|---|---|
| **Bridge 1** | 538 | 166 | 1456 | 1092 | 3.34 |
| **Bridge 2** | 523 | 149 | 2976 | 2232 | 11.47 |
| **Bridge 3** | 661 | 186 | 2565 | 1924 | 6.79 |
| **Bridge 4** | 529 | 210 | 2340 | 1755 | 5.84 |
| **Bridge 5** | 710 | 230 | 3885 | 2914 | 9.58 |
| | | | | Average | 7.40 |

## 3.4 Comparison of rating factors

The RFs from the STM are significantly higher than the sectional method, as expected, since the STM model captures the deep beam action. The results from the STM suggest that the total live load can be increased up to four times higher load, on average.

The RFs from the NLFEA are significantly higher than the STM, since the NLFEA considers many advanced material behaviors where concrete carries tension, and significant redistribution of the stresses, which provides extra capacity for the bridge bent beams. The STM, on the other hand, is a lower-bound method and terminates the analysis at the first yielding of rebar or first reaching the peak strain of concrete at any localized point. Based on the NLFEA result, these existing bridges can withstand, on average, seven times higher live loads combination.

The sectional method is not recommended for load rating of deep bridge bent beams, since it consistently provides overly conservative (i.e., lower capacity) results.

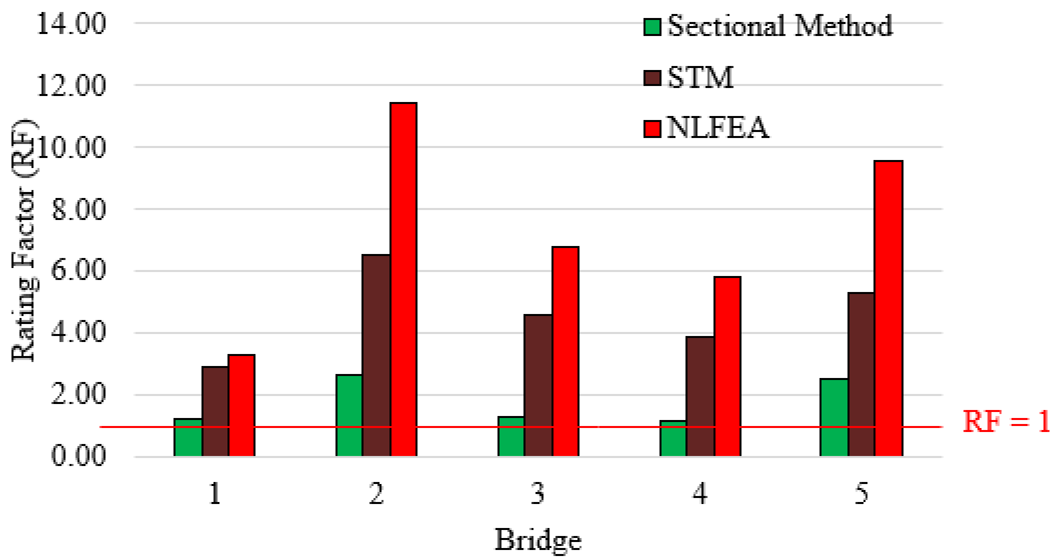


**Fig. 1**: Comparison of rating factors obtained from the sectional method, STM, and NLFEA.

## 3.5 Conclusions

Based on the rating factors (RF) determined from the sectional method, STM, and NLFEA for five existing bridges in Ohio, the following conclusions were made:

1. Analyses methods capable of representing the deep beam action can provide a better representation of the rating factor (RF).
2. The STM and NLFEA predict higher RFs for the deep bridge bents since they can capture deep beam strut action in bridges.
3. Using NLFEA for evaluating existing bridge bent beams will result in higher RFs and may reduce or eliminate the need for rehabilitation, significantly saving the owner cost.

## 3.6 Notations

C Capacity of member

*DC* Dead loads due to structural components

*DL* Dead load from one girder

$DL_t$ Total dead load acting on the beam

*DW* Dead loads due to wearing surface

*IM* Impact load due to live load

*LL* Live load from one girder

$LL_t$ Total live load acting on the beam

$\Phi$ Strength reduction factor

*P* Applied permanent loads other than dead loads

$P_f$ Failure load

RF Rating factor

# 4. System-Level Modeling Methodology for Helical Piles Foundation Systems Subjected to Uplift and Compression Loads.

This chapter includes the manuscript submitted to *Engineering Structures* journal by Anish Sharma and Serhan Guner. It is expected that there will be changes before the publication of the final paper. Please refer to the link https://www.utoledo.edu/engineering/faculty/serhan-guner/publications.html to download the final, published version of this paper.

## 4.1 Abstract

In tall and light structures, such as transmission towers, wind turbine, and light steel structures, there is an increasing application of helical pile foundation system to resist the uplift loading due to the wind. The uplift behavior of this foundation system depends on the interaction between structural components (i.e. helical piles and pile cap), and the soil. However, discrete modeling approaches are used by structural and geotechnical engineers to analyze them, which provide simplified idealization for the soil or a simplified idealization for the pile cap, respectively. As the interaction effects are neglected, the reliability of discrete modeling approaches in terms of uplift resistance of these foundation

systems is uncertain. To overcome this uncertainty, system-level experiments are highly desired, but they are expensive and difficult to perform, requiring an alternate method. This study proposes a system-level modeling methodology for the holistic analysis of helical pile foundation systems, accounting the effect of interactions as well as stress and strain nonlinearities inherent to the concrete and the soil. Important modeling considerations are discussed, and experimental benchmarks are provided to assist researchers in accurately performing holistic analyses. The effectiveness of the holistic analysis is discussed by comparing its results, including the load-displacement responses, load capacities, and failure modes with the discrete modeling approaches. Results demonstrated that discrete modeling approaches significantly underestimate the capacity up to 50%, and not accurately predict the failure modes, requiring a holistic analysis for these foundation systems.

## 4.2 Introduction

Helical Structures such as transmission towers and wind turbines are subjected to strong wind load, which creates uplift loading on their foundations. To resist this uplift loading, helical piles are commonly used due to their easy installation process, high tensile capacities, minimal noise, and vibration during installation, removability, reusability, cost-effectiveness, and suitability for areas with limited access (Perko 2009; Mohajerani et al. 2016). Helical piles are commonly made of high strength steel solid or hollow shaft, with helices fixed to the shaft at a specific spacing. These piles are installed in groups in the pile cap foundation system to obtain larger uplift load resistance, which depends on the linear and nonlinear behavior of the concrete and soil, and the interactions between the structural components (i.e. helical piles and pile cap), and the soil (Kwon et al. 2019; Guner and Carriere 2016; Young 2012; Fahmy and Naggar 2017; Sakr 2011; Haldar and Basu 2013; Mendoza et al. 2015). The structural analysis of helical pile foundation system usually uses a discrete modeling approach, in which there is limited consideration of the soil – pile – foundation interaction as the focus is on the capacity of the pile cap only. In this discrete approach, the piles are considered either as pinned or fixed supported and the soil mass is not considered (see Fig. 1a). On the other hand, the geotechnical analysis of this foundation system uses another discrete modeling approach where the soil and the helical piles are explicitly considered, but the interface of the piles – soil system with the pile cap is neglected and considered as pinned or fixed (see Fig. 1b). Both of these discrete modeling approaches oversimplify the actual behavior of the system, neglecting the effects of the interaction between the pile cap and the helical piles-soil system. Hence, a system – level modeling methodology considering all these components (see Fig. 1c) as well as the interaction between them is required for a more realistic simulation of the holistic behavior of the foundation system (Melendez et al. 2016; Uffe et al. 2012).

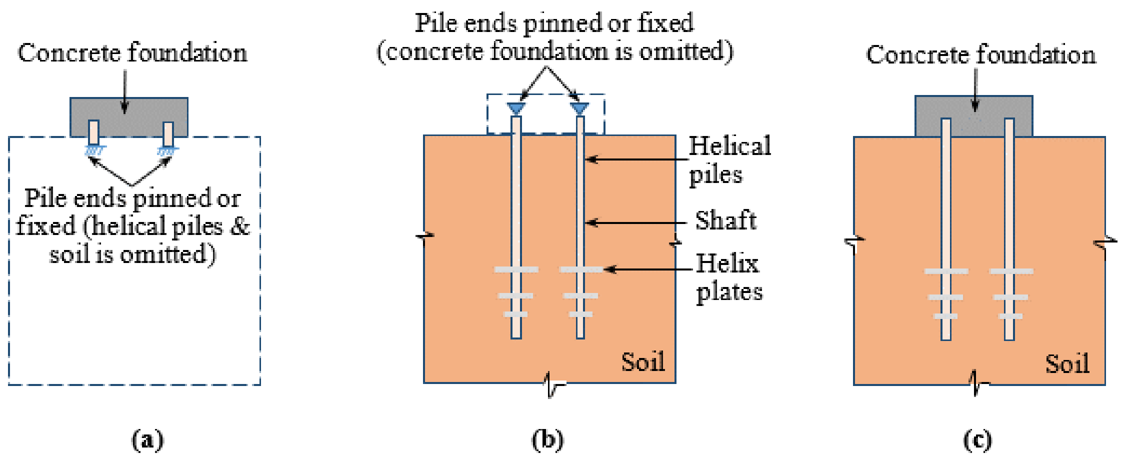


**Fig. 1.** Modeling approaches: (a) discrete foundation (structural modeling), (b) discrete helical piles & soil (geotechnical modeling), and (c) the proposed system-level model.

Despite the wide application and studies involving helical pile foundation systems, their holistic behavior has not been clearly established, which is critical for the accurate assessment of the uplift resistance of the entire system. The evaluation of the holistic behavior should include the nonlinearities and interactions between the soil, helical piles, and the pile cap, referred to as soil-pile-cap interaction (SPCI). To better understand the SPCI, full-scale experiments are highly desirable, but they are expensive and difficult to perform.

The current advancement in the computational capabilities of high-fidelity nonlinear finite element (NLFE) modeling has proven to be a versatile tool for studying the compressive behavior and the interactions between structural and geotechnical members (Hu and Pu 2003; Chen and Poulos 1993; Cao 2009; Suzuki and Otsuki 2002). Several studies employing NLFE modeling have accurately predicted the soil response using theories such as the Mohr-Coulomb, Drucker-Prager or Modified Drucker-Prager while employing contact elements with interactions defined by friction factors between the concrete (or steel) and soil (Suzuki et al. 2000; Elsherbiny and Naggar 2013; Labuz and Zang 2012; Alejano and Bobet 2012; Krenk 2000; Rawat and Gupta 2017; Salhi et al. 2013; Tan et al. 2008). Much fewer studies investigated the uplift behavior of helical piles and soil (Hu and Pu 2003; Salhi et al. 2013; Tan et al. 2008; Dib et al. 2019). Some of these studies employed two-dimensional (2D) finite element models (Labuz and Zang 2012; Alejano and Bobet 2012) while more recent ones presented three-dimensional (3D) finite element models to provide a more realistic simulation of the uplift behavior (Rawat and Gupta 2017; Salhi et al. 2013; Tan et al. 2008). These studies, however, present models applicable to certain conditions using certain computational modeling software.

This paper presents a 3D system-level modeling methodology for helical pile foundation systems, which can be applied to many soil and foundation conditions, while accounting for both soil and concrete nonlinearities as well as the soil-pile-foundation interactions. The proposed methodology does not require the use of any particular computer software because it calibrates the material and interaction properties with experimental benchmarks studies from the literature, which are also presented to assist researchers and practitioners in employing the proposed methodology. The methodology uses an experimentally-verified failure mechanism of the helical pile foundation system based on the relative displacement of the helical piles. The traditional, discrete modeling approaches (discussed above) are also employed to demonstrate how the response predictions compare with the proposed system-level modeling methodology in terms of the load-displacement responses, load capacities, and failure modes. In addition, numerical studies are performed to demonstrate the influences of critical parameters such as the soil conditions, number of helix plates, embedment depth of the helical piles inside the concrete foundation and the soil. While a special emphasis is places on load conditions creating net uplift loads (to bridge the current knowledge gaps), the applicability of the methodology to more traditional compression cases are also presented.

## 4.3 Proposed system-level modeling methodology

The proposed methodology uses three main stages as summarized in Fig. 2. These stages include: 1) verification of the behavior of the discrete pile cap (foundation) model, 2) verification of the behavior of the discrete helical piles & soil model, and 3) system – level modeling. The goal is to obtain the experimentally calibrated material and interaction models in Stages 1 and 2 using the experimental benchmarks to be presented below, such that an experimentally-verified system-level model could be created in Stage 3.

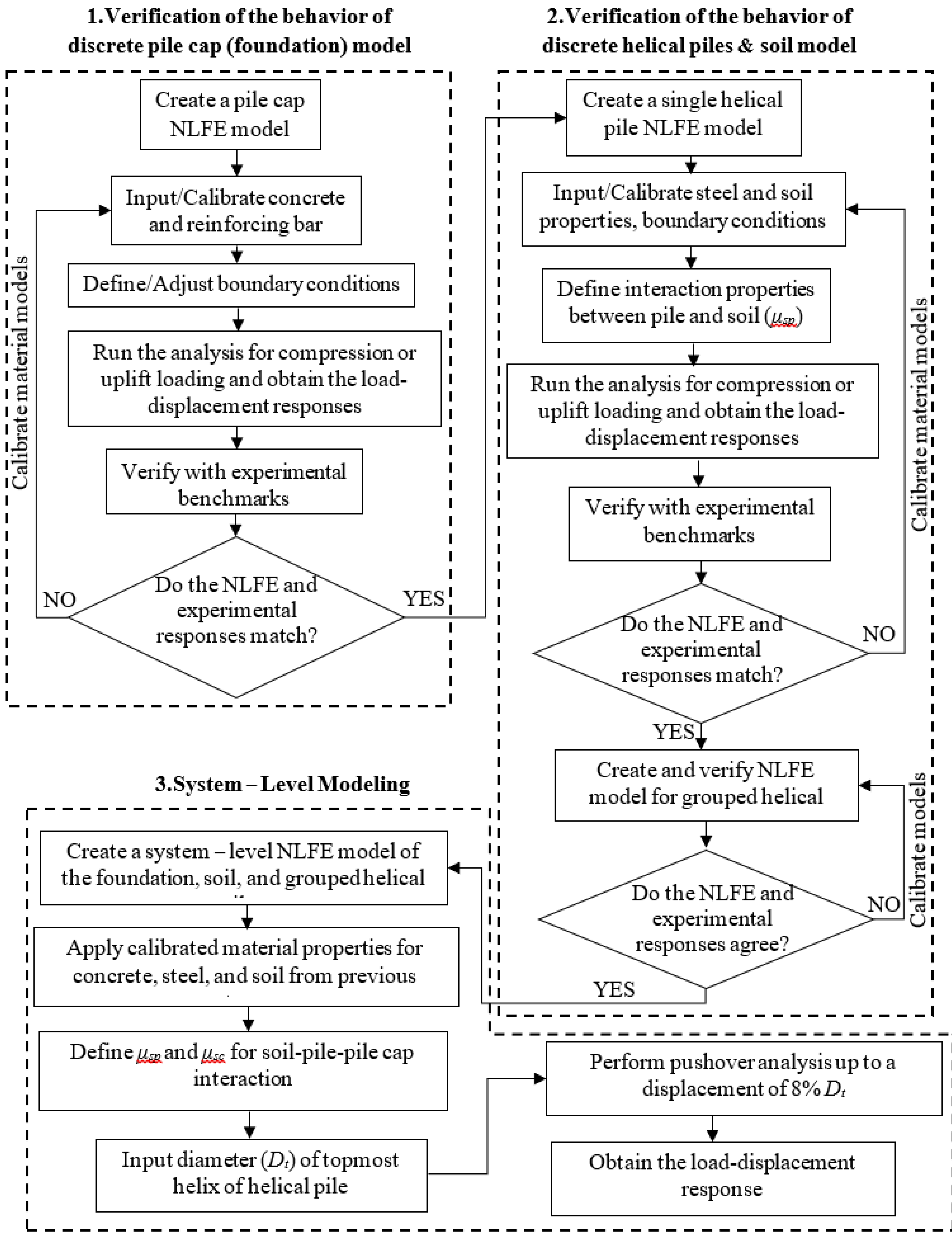


**Fig. 2.** Proposed system-level modeling methodology for helical pile foundation systems.

## 4.4 Verification of the behavior of discrete pile cap (foundation) model

The first stage of the proposed methodology requires the creation of a NLFE model for the discrete pile cap (discrete foundation). Symmetrical models are usually preferred because they tend to be more efficient. Any NLFE modeling software can be used, on the condition that it can simulate the nonlinear behaviors of materials and interaction properties through the calibration studies presented below.

The concrete damage plasticity (CDP) model, which is based on scalar plastic damage models proposed by Lee and Fenves (George et al. 2015), and Lubliner (Zhou et al. 2011) can be used as a constitutive model to simulate the inelastic compressive and tensile response of concrete (see Fig. 3a). The CDP model can also simulate the effects of the interactions between the concrete and reinforcing bars. Reinforcing bars are modeled as an elastic-plastic material, with the stress-strain response shown in Fig. 3b and are considered perfectly bonded to the concrete foundation.

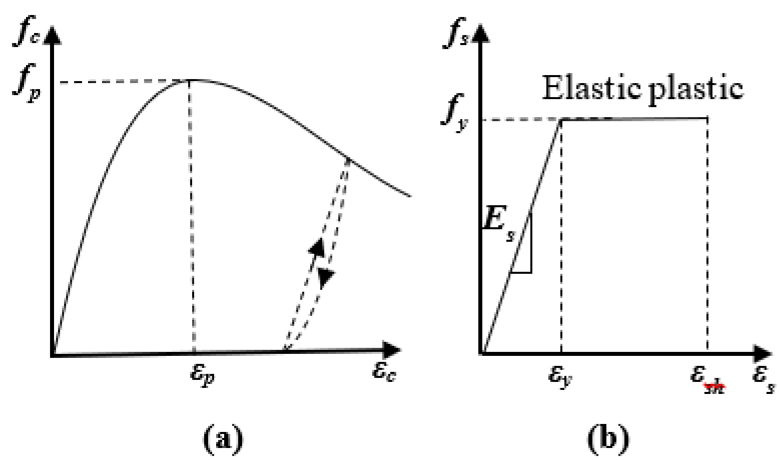


**Fig. 3.** (a) Concrete and (b) reinforcing bar constitutive models.

These material models have the capabilities to simulate the significant failure modes in a discrete foundation (Livneh and Naggar 2008; Cerato and Victor 2009), including punching shear (see Fig. 4a), one-way shear (see Fig. 4b), and flexural failures (see Fig. 4c).

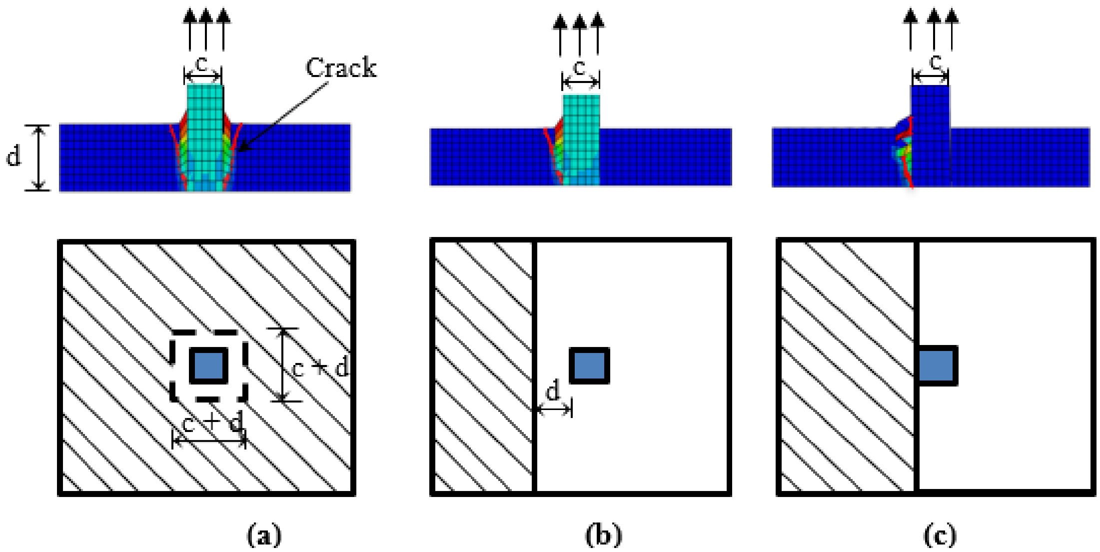


**Fig. 4.** Global failure modes for a discrete foundation: (a) Punching shear, (b) One-way shear, and (c) flexural failure.

After the material behaviors are defined, boundary conditions are applied at the support ends of the foundation, to prevent them from moving in any direction. If a symmetrical model is created, rollers should also be provided along the axis of symmetry. A pushover analysis is performed up to the failure of the foundation using a displacement-controlled loading protocol which permits the analysis to continue into the post-peak stages of the response, thereby showing the ductility and softening behavior of the foundation. At the end, the load-displacement response is obtained.

To verify the NLFE load-displacement response, experimental benchmark studies are conducted to assess the accuracy in terms of the initial stiffnesses, ultimate load capacities and the failure modes. In the case of a discrepancy (e.g., larger than $\pm$ 10%), the input material model properties should be adjusted, and the process is repeated until an adequate accuracy is obtained.

### 4.4.1 Experimental benchmarks for discrete pile cap (foundation) model

A number of suitable experimental benchmark specimens are selected from the literature, which can be used for the calibration of the NLFE material model while employing the proposed methodology. The specimens selected to exhibit predominantly shear and shear-compression types of failures because they are more challenging to capture (as compared to reinforcing-steel-governed flexural failures), and most foundations are deep concrete elements and pre-dominantly exhibit these types of failures. Both the compression and uplift load conditions are considered.

For the compression loading, the NLFE response can be verified with the experimental specimens tested by Vecchio and Shim 2004. This benchmark set includes twelve simply-supported beam strips of height 552 mm subjected to monotonic compression loads. Test results including load-displacement responses, load capacities, and failure modes are reported in detail (Vecchio and Shim 2004). The cross-sectional details, material properties, failure loads ($P_u$), and failure displacements ($\delta_u$) are presented in Table 1.

**Table 1** Experimental benchmark set details for discrete foundation modeling under compression (Vecchio and Shim 2004)

| Beam number | Length (mm) | Width (mm) | $f'_c$ (MPa) | $E_c$ (MPa) | Bottom rebar | Top rebar | Stirrups | $P_u$ (kN) | $\delta_u$ (mm) |
|---|---|---|---|---|---|---|---|---|---|
| VS-OA1 | 4100 | 305 | 22.6 | 36500 | 2 M30, 2 M25 | - | - | 331 | 9.1 |
| VS-OA2 | 5010 | 305 | 25.9 | 32900 | 3 M30, 2 M25 | - | - | 320 | 13.2 |
| VS-OA3 | 6840 | 305 | 43.5 | 34300 | 4 M30, 2 M25 | - | - | 385 | 32.4 |
| VS-A1 | 4100 | 305 | 22.6 | 36500 | 2 M30, 2 M25 | 3 M10 | D5 @ 210 | 459 | 18.8 |
| VS-A2 | 5010 | 305 | 25.9 | 32900 | 3 M30, 2 M25 | 3 M10 | D5 @ 210 | 439 | 29.1 |
| VS-A3 | 6840 | 305 | 43.5 | 34300 | 4 M30, 2 M25 | 3 M10 | D4 @ 168 | 420 | 51.0 |
| VS-B1 | 4100 | 229 | 22.6 | 36500 | 2 M30, 2 M25 | 3 M10 | D5 @ 190 | 434 | 22.0 |
| VS-B2 | 5010 | 229 | 25.9 | 32900 | 3 M30, 2 M25 | 3 M10 | D5 @ 190 | 365 | 31.6 |
| VS-B3 | 6840 | 229 | 43.5 | 34300 | 3 M30, 2 M25 | 3 M10 | D4 @ 152 | 342 | 59.6 |
| VS-C1 | 4100 | 152 | 22.6 | 36500 | 2 M30 | 3 M10 | D5 @ 210 | 282 | 21.0 |
| VS-C2 | 5010 | 152 | 25.9 | 32900 | 2 M30, 2 M25 | 3 M10 | D5 @ 210 | 290 | 25.7 |
| VS-C3 | 6840 | 152 | 43.5 | 34300 | 2 M30, 2 M25 | 3 M10 | D4 @ 168 | 265 | 44.3 |

Sectional areas: M10 = 100 mm$^2$; M25 = 500 mm$^2$; M30 = 700 mm$^2$; D4 = 25.7 mm$^2$; D5 = 32.2 mm$^2$.

If there is a load case involving net uplift loading, the NLFE response can be calibrated with the experimental specimens tested by Diab (2015). This benchmark set includes seven discrete pile cap strips of dimensions 500 x 500 x 1600 mm subjected to uplift loading. Test results including load-displacement responses, load capacities, and failure modes are reported in detail (Diab 2015). Uplift loading is applied by pulling the specimens with two embedded steel piles of varying depths ($d_e$). The material properties, failure load ($P_u$), and failure displacement ($\delta_u$) are shown in Table 2.

**Table 2** Experimental benchmark details for discrete foundation modeling under uplift (Diab 2015)

| Beam num. | $f'_c$ (MPa) | Top & Bottom rebar | Stirrups | $d_e$ (mm) | $P_u$ (kN) | $\delta_u$ (mm) |
|---|---|---|---|---|---|---|
| T1 | 30 | 4-15M | 2-#2 @ 200 | 152 | 154.0 | 2.5 |
| T2 | 30 | 4-15M | 2-#2 @ 200 | 203 | 201.0 | 3.6 |
| T3 | 30 | 4-15M | 2-#2 @ 200 | 254 | 232.0 | 2.0 |
| T4 | 40 | 4-20M | 2-#2 @ 200 | 203 | 222.5 | 1.3 |
| T5 | 40 | 4-25M | 2-#2 @ 200 | 203 | 252.3 | 1.0 |
| T6 | 40 | 4-15M | 4-#2 @ 200 | 203 | 256.3 | 6.4 |
| T7 | 40 | 4-15M | 2-#2 @ 200 | 203 | 253.2 | 2.7 |

Sectional areas: M15 = 200 $mm^2$; M20 = 300 $mm^2$; M25 = 500 $mm^2$; #2 = 32 $mm^2$.

The calibrated material model inputs that yield acceptable response simulations with the experimental benchmark sets are recorded for use in Stage 3 when creating a system-level model.

## 4.5 Verification of the behavior of discrete helical piles & soil model

The second stage of the proposed methodology requires the creation of a NLFE model for the discrete helical piles & soil model through a two-step process: first for a single helical pile, and then for a grouped helical pile.

The single helical pile, made up of steel material, is modeled with an elastic-plastic constitutive model as shown in Fig. 3b. The soil is modeled with an elastic-plastic constitutive model with a failure mode governed by the Mohr-Coulomb criteria (Sun et al. 2006). If the shear stress ($\tau$) is greater than $c + \sigma \tan \Phi$, where $c$ is the cohesion, $\Phi$ is the friction angle of soil, and $\sigma$ is the normal stress, the soil fails as shown in Fig. 5a. This failure criterion is used for its simplicity and extensive applicability for complex soil-structure interaction analysis as demonstrated elsewhere (Sun et al. 2006). Two independent material parameters (Young's modulus, *E, and* Poisson's ratio, *v*) define the state of the isotropic linear-elastic properties of the soil. The model allows the representation of nonlinear behavior of the soil based on the prescribed variations of the Mohr-Coulomb model properties, namely: cohesion, friction, dilation. Furthermore, this material model is capable of simulating two primary failure modes: individual plate uplift where the failure occurs above all of the helical plates (see Fig. 5b), and cylindrical shear where a more global failure occurs through the plate and the soil act together as a cylinder (see Fig. 5c).

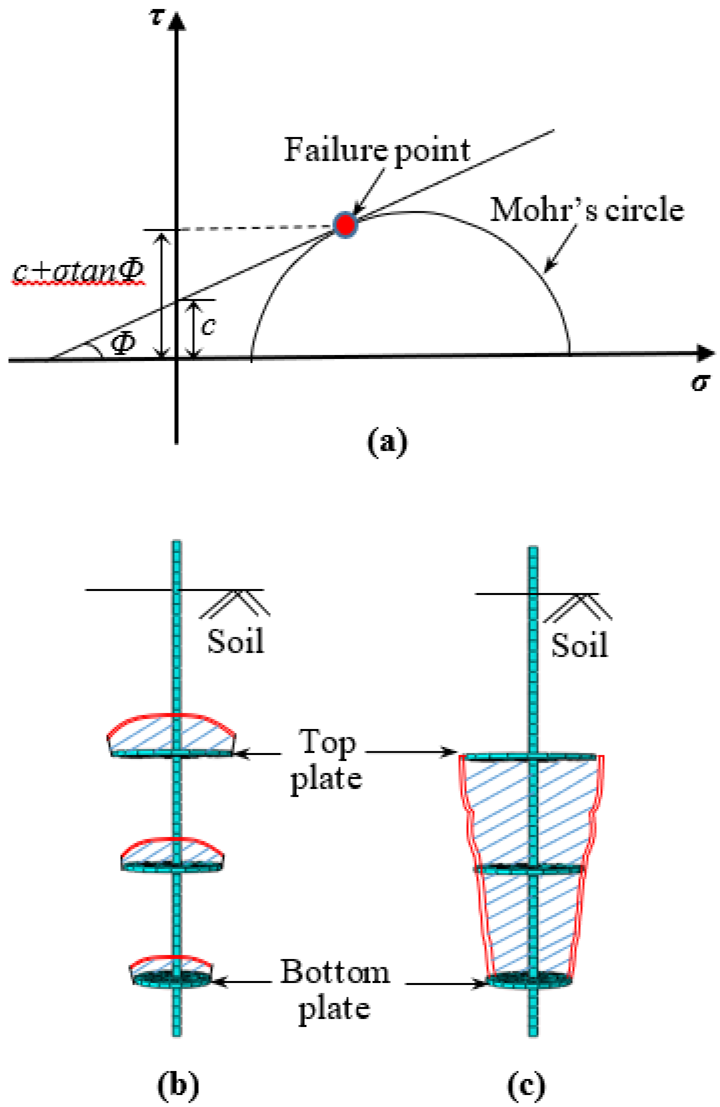


**Fig. 5**. (a) Constitutive model for the soil, failure model for helical pile-soil (b) individual plate bearing, and (c) cylindrical shear.

The main objective of Stage 2 is to obtain the experimentally calibrated interaction model to simulate interface between soil and the piles. The typical soil deformations that occur in soil-pile interactions include plastic flow, expansion (dilation) that can occur with shear deformation, soil compaction, and soil distortion. These interactions in the interface between the pile cap, helical piles, and the soil depend on the friction angle and the adhesion. For deep helical piles, the contribution of the friction along the pile shaft can be substantial. In the proposed methodology, the interaction behavior between soil and pile is defined with an experimentally-calibrated coefficient of friction between the interface elements. The friction between the two surfaces in contact depends on the material properties of the surfaces. In the absence of geotechnical investigation results, common soil-structure friction factors from NAVFAC standards are presented in Table 3.

**Table 3** Interface properties of different materials (NAVFAC 1982)

| **Interface materials** | | **Friction factor** | **Friction angle** |
|---|---|---|---|
| Concrete | Rock | 0.70 | 35 |
| | Gravel | 0.55-0.60 | 29-31 |
| | Medium sand | 0.35-0.45 | 19-24 |
| | Stiff clay | 0.30-0.35 | 17-19 |
| Steel | Gravel | 0.40 | 22 |
| | Silty sand | 0.25 | 14 |
| | Fine sandy slit | 0.20 | 11 |

To define the boundary conditions in the discrete helical piles & soil model, the bottom of the soil is fixed in all direction and the sides are constrained in the horizontal direction. A displacement-controlled axial loading is applied at the top of the helical piles while the helix plate displacements are recorded. The load-displacement response is obtained for verification with the experimental benchmark studies to assess the accuracy in terms of the initial stiffness, the ultimate capacity & displacement, and the failure mode. In the case of a discrepancy (e.g., larger than + 10%), the input material and interaction properties should be adjusted, and the process is repeated until an adequate accuracy is obtained. Once the single helical pile response is verified, a model of grouped helical piles is created and verified in a similar manner.

### 4.5.1 Experimental benchmarks for single and grouped helical pile – soil model

A number of suitable experimental benchmark specimens are selected from the literature, which can be used for the calibration of the NLFE model while employing the proposed methodology. The geometric details and the soil properties are presented in Fig. 6 and Table 4, respectively. For the single pile model, the NLFE response can be verified with four experimental specimens (SP1, SP2, SP3, and SP4) tested by Gavin et al. 2014, Sakr 2013, and Livneh and Naggar 2008. For the group helical piles model, the NLFE response can be verified with the experimental specimens (GP1) tested by Lanyi and Deng 2018. These selected specimens exhibit predominantly cylindrical shear failure that follows the tapered profile of the inter-helices soil in the direction of loading, and most helical pile foundations exhibit these types of failure. Test results including load-displacement responses, load capacities, and failure modes are reported in detail (Gavin et al. 2014; Sakr 2013; Livneh and Naggar 2008; Lanyi and Deng 2018). The properties of the soil are provided and classified using the soil class defined by the united soil classification system (USCS) standards (Howard 1984). The available data is sufficient to model the soil using Mohr-Coulomb's criteria, as discussed in the proposed methodology.

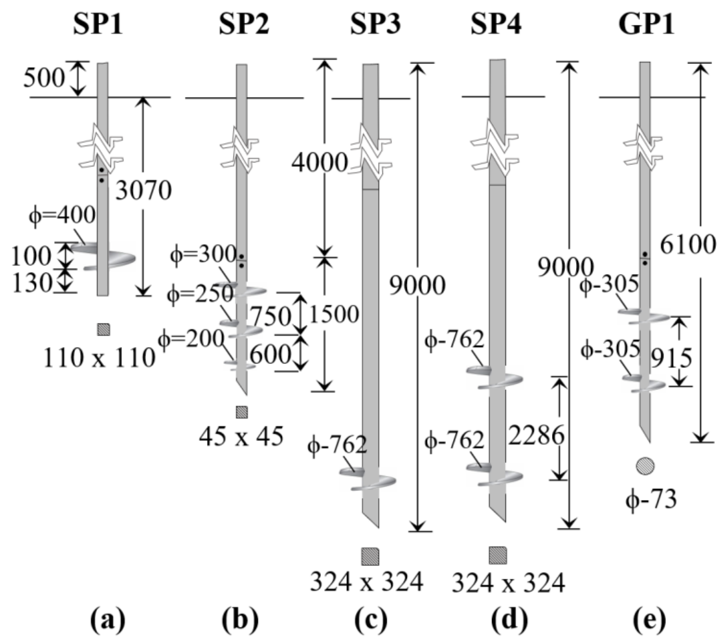


**Fig. 6.** Geometrical details (dimensions in mm) of helical piles experimental benchmarks (a) SP1, (b) SP2, (c) SP3, (d) SP3, and (e) GP1.

**Table 4** Soil properties for benchmark helical pile specimens

| **Specimens** | **E (MPa)** | **Φ (º)** | **ψ (º)** | **c (kPa)** | **Soil Type (USCS )** |
|---|---|---|---|---|---|
| SP1 | 23 | 56 | 33 | 0 | GW |
| SP2 | 54 | 28 | 0 | 10 | OL |
| SP3 | 48 | 35 | 5 | 1 | GM-GL |
| SP4 | 48 | 35 | 5 | 1 | GM-GL |
| GP1 | 50 | 22* | 0 | 25 | CH |

*Estimated based on USCS soil class (Howard 1984)

## 4.6 System – level modeling

The system – level model of helical pile foundation systems is created based on the experimentally-calibrated material and interaction models obtained from Stages 1 and 2 discussed above. When creating a system – level model (e.g., Fig. 7a), the main consideration should be given to how soil – structure interface are defined between the soil and concrete foundation (denoted with subscript sc), and soil and helical piles (denoted with subscript sp). In this study, these interactions are defined with pair of contact elements as shown in Fig. 7b. This interaction model is based on the Coulomb law of friction and depends on the coefficient of friction ($\mu_{sc}$ or $\mu_{sp}$) between two surfaces in contact (see Fig. 7c).

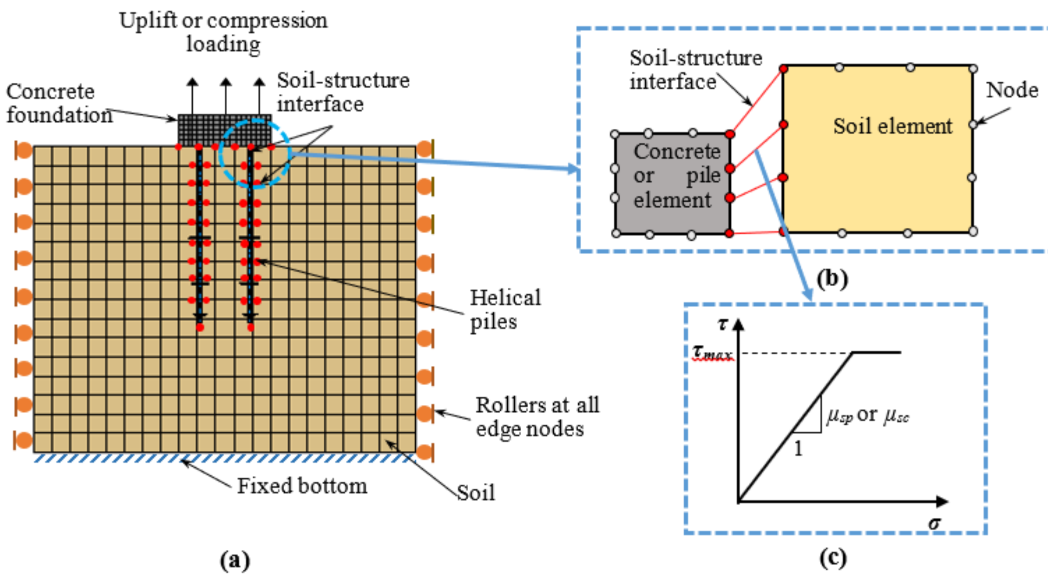


**Fig. 7.** (a) A sample system-level FE model, (b) modeling soil-structure interface, and (c) interaction model at the interface.

When defining the boundary conditions, a special attention should be paid to ensure that that the variations in the strain profile is contained within the modelled soil area which shows that the model of the soil mass is sufficiently large. A displacement-controlled loading is desired, as opposed to a force-controlled one, at the top of the concrete foundation (see Fig. 7a), in a monotonically increasing manner until the failure. Displacement control will allow the analysis to continue in the post-peak region allowing the quantification of the deformation capacity of the system and identification of the failure mode. The Mohr's Coulomb failure criterion with an 8% displacement cut-off (i.e., 8% of the topmost helix plate diameter, $D_t$) is found to successfully capture the experimental responses considered in this study. Similar failure criteria ranging from 5% to 10% of lead helix (top helix) diameter are also found suitable in other studies (e.g., Elsherbiny and Naggar 2013; Livneh and Naggar 2008). At the end of the analysis, a system – level load-displacement response is obtained from which the stiffness, peak load capacity, and the displacement ductility can be obtained. The failure mode of the system should be determined using the deformed shape, stress and strain contours and the post – peak stages of the load displacement response.

## 4.7 Application of the system – level modeling methodology

In this section, numerical studies are presented to illustrate the application of the proposed methodology for performing system – level modeling of two helical piles group foundation system embedded in silty sand (i.e. 50% of the coarse fraction passes 4.75 mm sieve). The geometric and material details of discrete components (i.e. concrete foundation, steel helical pile, and the soil) of the sample system to be modelled is shown in Fig. 8.

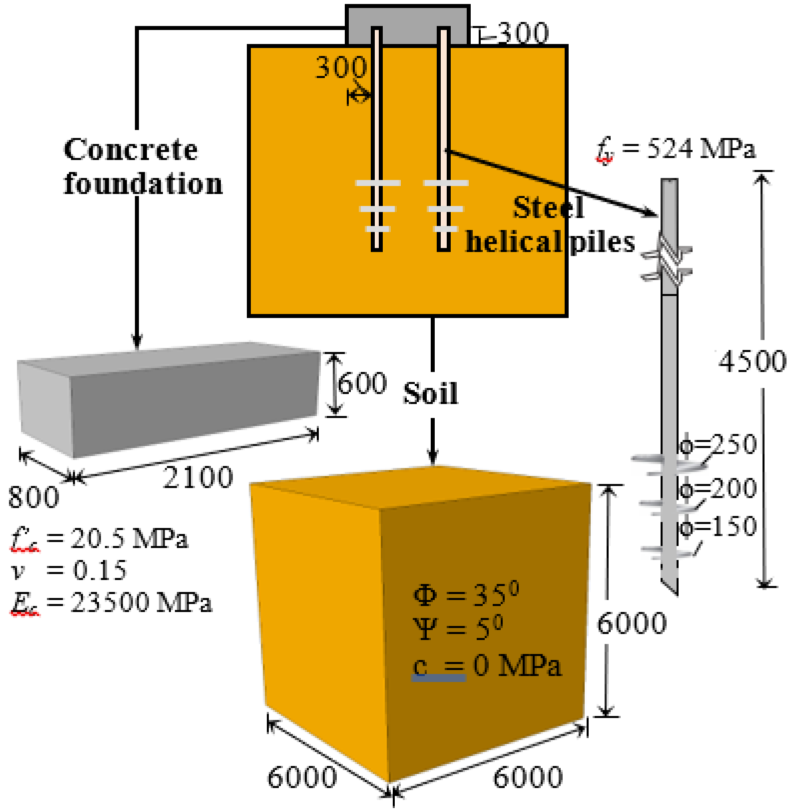


**Fig. 8.** Geometric details (dimensions in mm), material properties, and modeling setup for the system-level modeling.

The proposed methodology requires that a discrete concrete foundation model is created and experimentally verified first. While the Abaqus v6.14 program is used in this study, any other NLFE modeling program can be used, on the condition that it can capture the responses of the experimental benchmark specimens. In Stage 1, the material properties, interaction properties, and boundary conditions for concrete foundation model is defined as discussed in Section 2, and the model will be calibrated for both compression and uplift loads for demonstration purposes. The compression load verification is conducted using the experimental benchmarks (VS-OA1, VS-OA2, and VS-A3) subjected to mid-span displacements. The complete load-deflection responses (see Fig. 9a) and the failure modes (see Figs. 9b, 9c, and 9d) are obtained and compared with the experimental results. Von mises stresses indicate if the material will yield or fracture. It is not appropriate for brittle materials like concrete but illustrated in this study to visualize how stresses are distributed in the discrete foundations. Strains would be relatively good representation of damage pattern; hence plastic strain distributions of the concrete model are compared with the experimental cracking patterns to validate the failure mode. The discrepancy between the FE simulation and experimental values of the peak load capacities are found on be less than 10%, indicating the successful calibration of the material model parameters, as shown in Table 5, where fbo/fco is the ratio of initial biaxial compressive yield stress to the initial uniaxial compressive yield stress, and K is the ratio of the second stress invariant on the tensile meridian to that on the compressive meridian (ABAQUS 2014). It should be emphasized that the benchmark specimens should be carefully selected to incorporate the expected behaviors. The specimens VS-OA1 and VS-OA2 used in this study contained no shear stirrups, similar to the foundation modelled, and failed in diagonal tension and shear dominated failure modes.

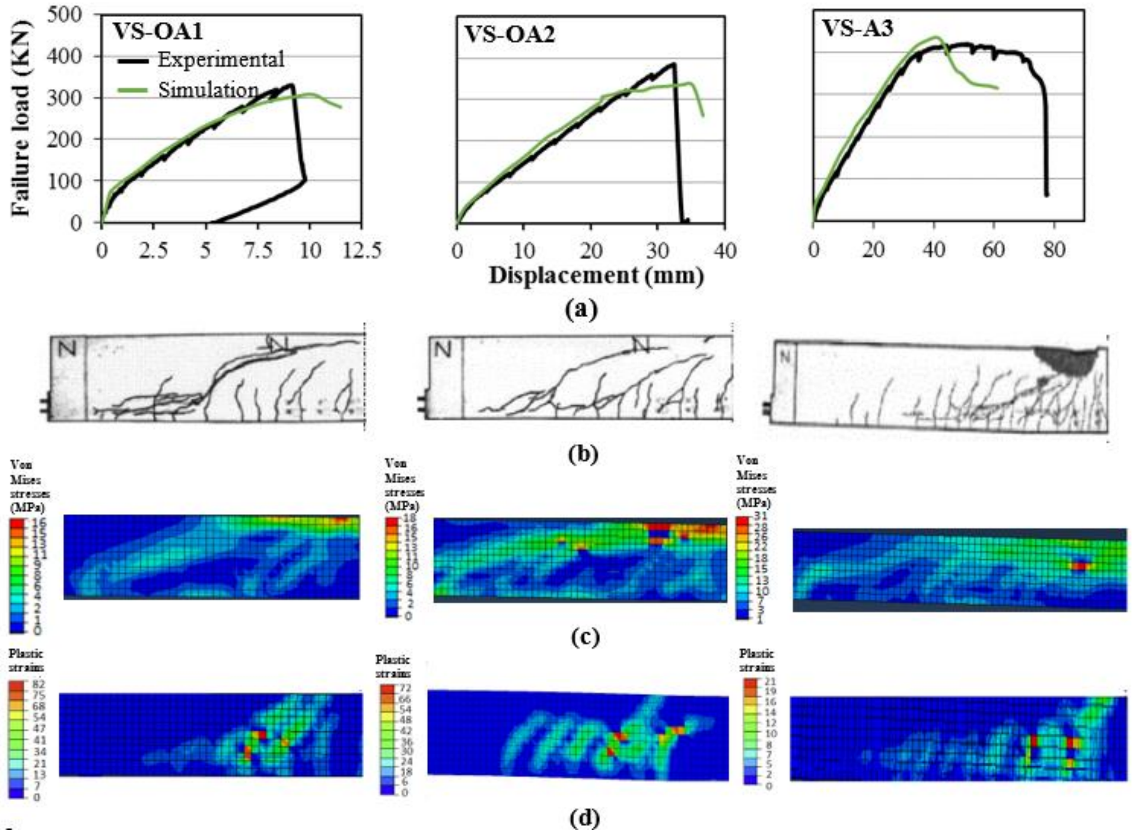


**Fig. 9.** (a) Load-displacement response, (b) experimental failure mode, (c) captured stresses distribution, and (d) cracking pattern from FE simulation under compression load.

**Table 5** Concrete damage plasticity input parameters for Stage 1 concrete under compression

| **Parameter** | **Value** |
|---|---|
| Dilation angle *($\psi$)* | 35 |
| Eccentricity ($\epsilon$) | 0.1 |
| $fb_o/fc_o$ | 1.16 |
| $K$ | 0.667 |
| Viscosity ($\mu$) | 0.0001 |

A similar process is employed for the uplift loads using the benchmark Specimen FT1 (see Table 2). The results of the experimental verification study are presented in Fig. 10 in terms of load-displacement response and failure modes. The calibrated material model input is presented in Table 6.

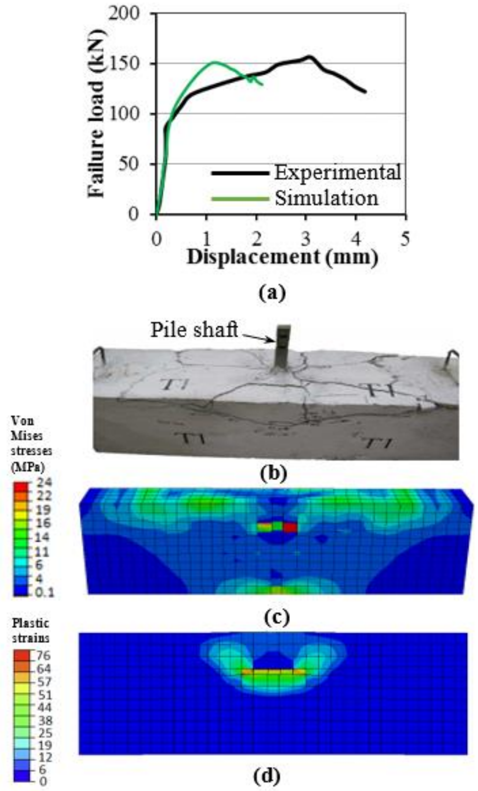


**Fig. 10.** (a) Load-displacement response, (b) cracking conditions from experiments, (c) stress distribution and (d) cracking condition from FE simulation, for discrete foundation under uplift.

**Table 6** Concrete damage plasticity inputs for concrete under uplift

| Parameter | Value |
|---|---|
| Dilation angle $(\psi)$ | 37 |
| Eccentricity $(\epsilon)$ | 0.1 |
| $fb_o/fc_o$ | 1.16 |
| $K$ | 0.667 |
| Viscosity $(\mu)$ | 0.0001 |

In Stage 2, a discrete helical pile & soil model is created (see Fig.11a) through a two-step process. The first step is to model and experimentally verify a single helical pile model while the second step involves modeling and verifying the grouped helical pile system (incorporating the calibrated single pile models) to obtain the calibrated material and interaction properties. For the first step, the material properties and boundary conditions are defined as discussed in Section 2. To simulate the interaction between soil and helical pile, the master-and-slave surface approach with hard contact is adopted, which is defined with the coefficient of friction obtained from Table 3. Pushover analyses are performed to obtain the load-displacement responses for comparison with the experimental results. For the second step, the grouped helical pile system (GP1) is created and the material models are calibrated, following a similar procedure. The captured load-displacement responses and failure mode for the experimental benchmarks (SP1, SP3, SP4, and GP1) matches and are illustrated in Fig. 11. Von mises stresses distribution of the helical pile & soil model is used for predicting the load transfer and failure mechanisms (Kwon et al. 2019), assuming the soil under plastic yielding. The discrepancy between the FE simulation and experimental values of the peak load capacities are found on be less than 10%, indicating the successful calibration of the soil model using Mohr' coulomb model and interaction model parameters.

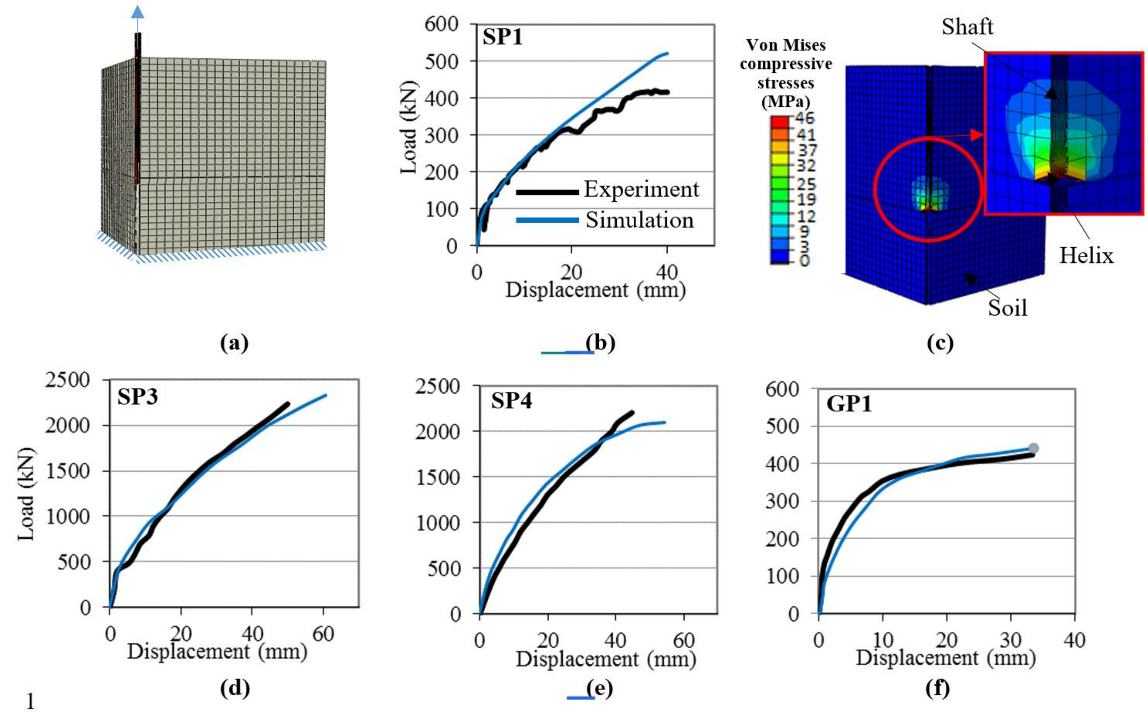


**Fig. 11.** (a) Discrete single helical pile & soil NLFE model, (b) load-displacement response, (c) soil stresses distribution at failure load, and load-displacement responses for (d) SP3, (e) SP4, and (f) GP1.

In Stage 3, a system-level model is created, as shown Fig. 7a, using the eight-nodded, first-order, and reduced-integration continuum solid elements (C3D8R). The experimentally calibrated material models for the concrete, and the soil obtained from Stage 1 and Stage 2 are employed. The interaction between soil and piles were considered as hard contact, as it minimize the penetration of soil surface into the pile and does not allow the transfer of tensile stress across the interface, with a coefficient of friction ($\mu_{sp}$) of 0.2, and also the interaction between soil and pile cap as hard contact with a coefficient of friction ($\mu_{sc}$) of 0.35, following Table 4. The appropriate support conditions are applied and a displacement-controlled pushover analyses is performed for both the compression and uplift load cases.

The load-displacement response of the system, shown in Fig. 11b, exhibits three distinct regions: initial linear-elastic region with a high stiffness, non-linear hardening region, and plastic yielding and failure region shown in Fig. 12b. The first region represents the shaft friction while the second one represents the stress distribution to the soil around the pile shaft and helices. The failure corresponding to 8% of topmost helix diameter of 250 mm occurs between at the transition from the second to third regions with and an uplift capacity of 610 kN. The stress distribution shown in Fig. 12a demonstrates that the soil failure occurred above the topmost helix through the formation of a soil cone. In this cone, the shear stress exceeds the shear strength of the soil, causing the soil element to fail above the topmost helix. The interface element between the concrete foundation and the soil contributes to the redistribution of the stresses, causing a reduction in the resisting forces at ends of the helical piles, ultimately increasing the load and displacement capacities. The concrete foundation showed local cracking but did not fail, as the stresses gets distributed uniformly on the interface between the foundation and the soil.

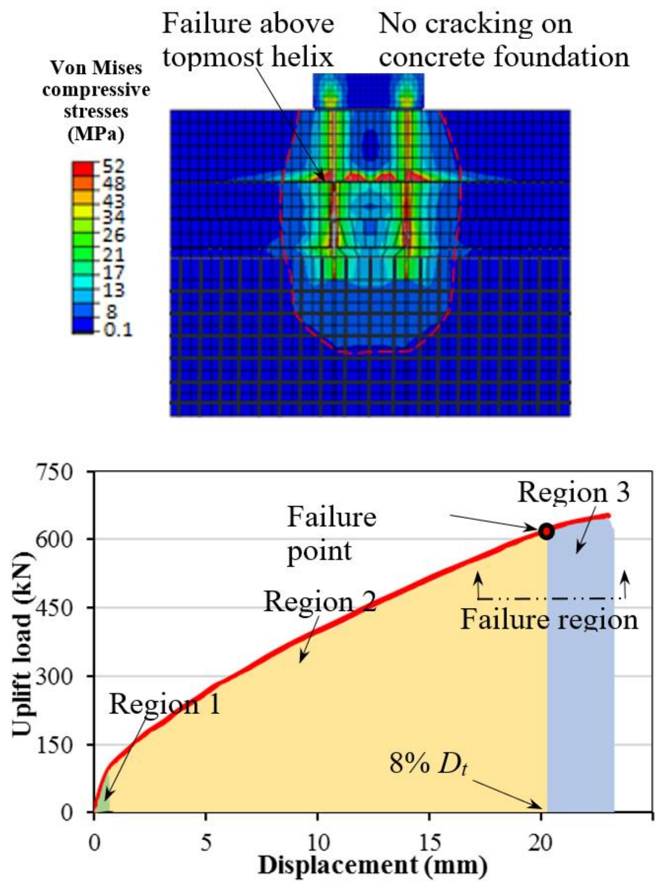


**Fig. 12.** (a) Stresses distribution, and (b) load-displacement response for the system-level model at 20 mm displacement (i.e. 8% $D_t$).

## 4.8 Comparison of discrete models with the system – level model

To demonstrate how the traditional discrete modeling results, compare with those from the proposed system-level modeling methodology, the discrete pile cap and the discrete helical piles & soil model are created, as shown in Fig 13. The results are examined in terms of the load capacities and the failure modes.

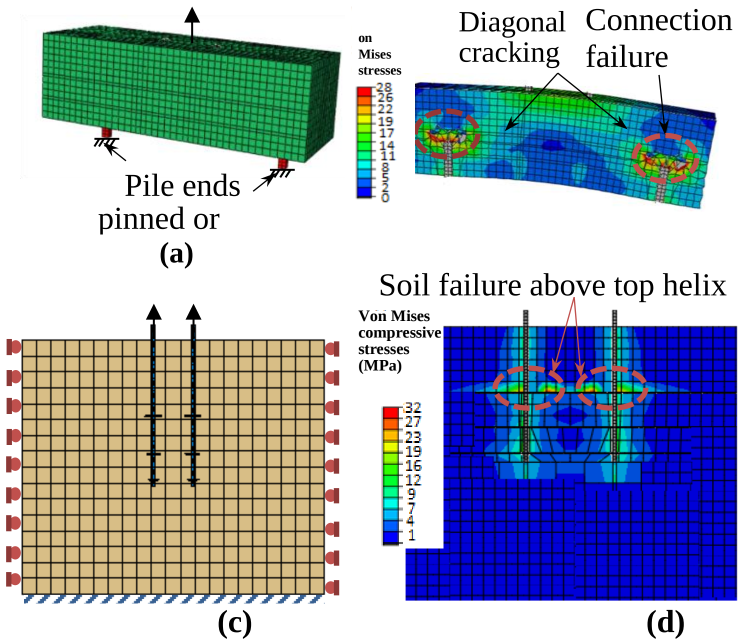


**Fig. 13.** Comparison between discrete and system – level models in-terms of failure modes and load capacities.

In the discrete pile cap model (see Figs. 13a and 13b), diagonal shear cracking occurred in the pile cap which eventually led the failure to form around the pile cap termination bracket. Hence, the uplift capacity of the discrete model was found to be 450 kN. In the discrete helical piles & soil model (see Fig. 13c), the failure mode was in the soil above the topmost helix as shown in Fig. 13d, similar to system-level model, with a capacity of 450 kN. Note that both system components are intentionally designed for the same load capacity to allow for a consistent comparison with the system-level models. The capacities obtained from all three models are presented in the load-displacement response shown in Fig. 14 which shows that the discrete models underestimate the load capacity by 26%. The load sharing and interaction between the system components permits the re-distribution of stresses, allowing for larger load and displacement capacities to be achieved.

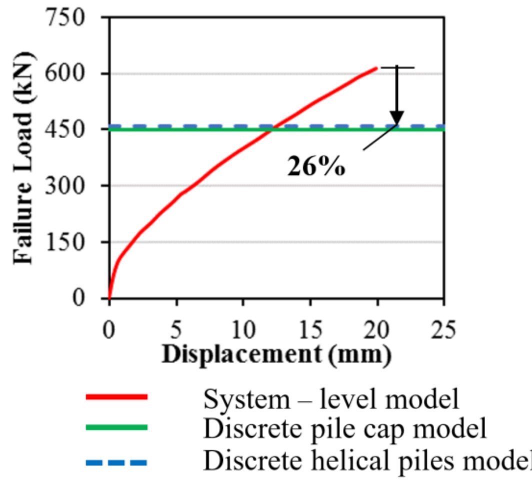


**Fig. 14.** Uplift capacities comparison from system – level and discrete models.

## 4.9 Influence of soil type on the system – level model

To demonstrate the significance of the soil type, two more system-level models are created using organic clay (OL) and well-graded gravel soil (GW) as shown in Table 7. Soil types are selected to represent from soft to stiff conditions following USCS soil classification.

**Table 7** Soil parameters as per USCS soil class

| USCS Soil-class | Description | c (kPa) | Φ (°) | Remarks |
|---|---|---|---|---|
| GW | Well-graded gravel | 0 | 40 | stiffer |
| GM-GL | Silty gravel | 0 | 35 | |
| OH | Organic clay, organic silt | 10 | 22 | soft |

The simulated load-displacement responses are presented in Fig. 15, along with the capacity lines obtained from the discrete models. The results indicate that stiffer soil significantly increases the capacity of the system-level models. The discrete models underestimated the system capacity in all cases. An important conclusion is that as the soil gets stiffer, the discrete modeling assumption of pile cap becomes more realistic and the result converges.

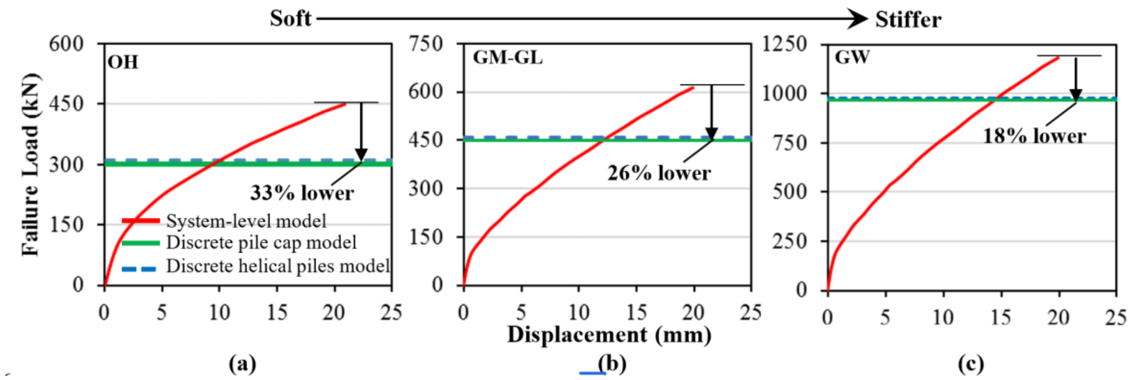


**Fig. 15.** Influence of different soil types on the system-level model and discrete models for (a) OH soil class, (b) GM-GL soil class, and (c) GW soil class as per USCS.

## 4.10 Influence of various design configurations

To investigate the influence or various design configurations and draw conclusions on which of design parameter are significant in the holistic system design for uplift loads, additional numerical studies are performed as discussed below.

### 4.10.1 Pile embedment in the concrete pile cap

A holistic analysis is performed to estimate the ultimate capacities with different embedment depths of the helical pile termination brackets inside the pile cap. The simulations are performed in three embedment depth conditions: top (T): 550 mm, middle (M): 300 mm and bottom (B): 50 mm – all measured from the bottom of the pile cap (see Fig. 16a). The system-level uplift capacities obtained are plotted in Fig. 16b. The increase in the embedded distance inside the pile cap from bottom to middle increases the uplift capacity by 25%. This conclusion is in agreement with the findings published elsewhere (Guner and Chiluwal 2019; Chiluwal and Guner 2019). By further increasing the embedment depth from middle to the top, the uplift capacity only increases by 8%. The use of bottom embedment depth resulted in pre-mature cracking of concrete around the connection; the failure occurred in these zones by the detachment of the helical piles from the pile cap. Hence middle embedment depth inside the pile cap is recommended for helical pile system.

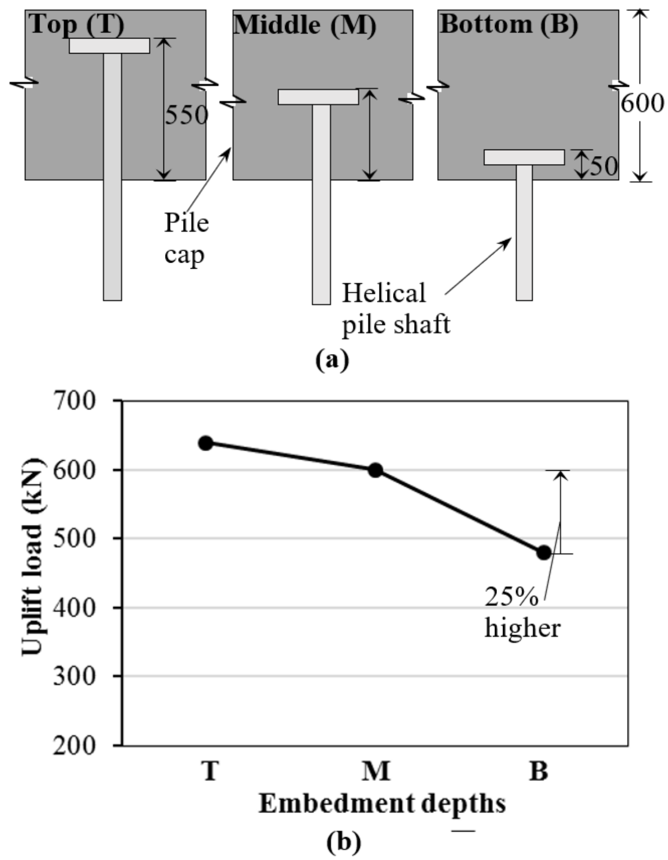


**Fig. 16.** (a) Geometric details (dimensions in mm) of pile shaft embedment depths, and (b) uplift capacities response with embedment depths.

## 4.10.2 Pile embedment in the soil

Embedment depth is defined as the distance from the top helix plate to the ground surface. System-level model with three helices helical piles are analyzed with varying soil embedment depths from 4000 mm to 5000 mm. The embedment in the concrete pile cap is fixed for 300 mm (termed as the middle embedment). The uplift capacities obtained are shown in Fig. 17a. The uplift capacity increases by 18% if the pile embedment in the soil is increased from 4000 mm to 4500 mm. On further increasing the embedment depth by 500 mm, the capacity gain is similarly found to be 16%. With the increase in the pile embedment in the soil, the initial linear segment of the load-displacement curve becomes stiffer, which contributes to the increase in the capacity of the system-level model.

### 4.10.3 Helices number

The number of helices attached to the helical pile shaft is varied between single, double and triple. The load-displacement curves are shown in Fig. 17b. The uplift capacity of helical pile is found to increase by 36% as the number of plates increases from single to double, where the soil between two helix plates act as a solid mass and provide extra capacity. By increasing helix plate number from double to triple, the increase in the load capacity is found to be a smaller value of 18%.

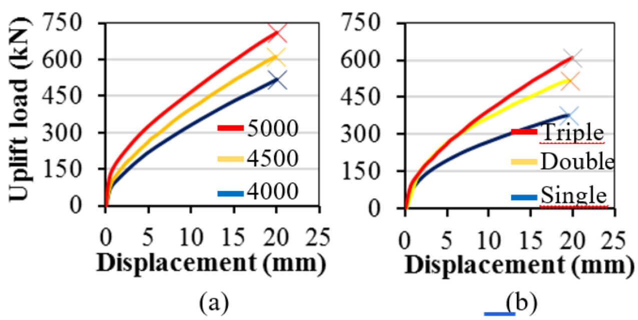


**Fig. 17.** Influence of (a) pile embedment inside the soil, and (b) pile embedment in the pile cap in uplift capacity prediction from the system-level holistic analysis.

## 4.11 Conclusions

A methodology is proposed for the system – level analysis of helical pile foundation systems accounting for both soil and concrete nonlinearities as well as the soil-pile-foundation interactions using the experimentally-verified failure mechanism based on relative displacement of the helical pile. The effectiveness of the methodology is demonstrated by comparing its results with discrete modeling approaches. In addition, the influence of soil type and various design configurations of helical piles on holistic behavior prediction under uplift loading was investigated. From this study, the following inferences are made.

- The traditional discrete modeling approaches has significant shortcoming in capturing the failure modes and the load capacities of the helical pile foundation systems. The influence of soil is neglected during the structural pile cap modeling while the influence of the concrete pile cap is neglected during the helical pile and soil modeling.
- As compared to the system-level model including all system components, the discrete modeling approach underestimated the load capacities by up to 33% under uplift. These large discrepancies between the discrete and system-level modeling approaches are obtained in softer soils.
- The load capacity predictions from the discrete and system-level modeling approaches converges as the soil becomes stiffer because the discrete modeling assumption of fixed boundary conditions become more realistic in stiffer soils.
- The system-level models demonstrate that the location of the helical pile termination bracket inside the concrete pile cap has a significant influence on the uplift capacity of

the entire system. The bottom embedment depths resulted in premature concrete cracking at connection zone – a concern for long-term durability due. The systems incorporating bottom embedment depths failed at load capacities 25% less than those obtained from middle embedment depths. This type of failure is not considered in the traditional discrete modeling approaches.

- A well-defined 3D modeling methodology is proposed to better understand the holistic behavior of the helical pile foundation systems and more accurately quantify their load and displacement capacities, and visualize the system-level failure modes, including the premature and undesirable ones.
- The proposed methodology uses experimentally calibrated material models without requiring the use of any specific computer programs on the condition that it can capture the significant failure mechanisms demonstrated in this study. Experimental benchmark sets and how the calibration process is conducted is also defined in this study.
- The methodology uses a failure criterion based on the relative displacement of helices in the helical pile. Experimental failure reported in literatures occurred mostly when the load-displacement curve reaches a displacement equivalent to 8% of topmost helix plate diameter.
- With the increase in helical plate numbers, the pile embedment depths inside the soil and the pile cap, higher resistance is developed from shaft friction in the system-level model, ultimately increasing the uplift resistance up to 36% in the case studied.

# 5. Conclusions

In this study, two methodologies on numerical modeling of the deep concrete members are presented. Based on the research results obtained, the following conclusions are drawn.

### For deep bridge bent beams,

- Most bridge bents are deep beams with nonlinear strain distributions. Analysis methods capable of representing the deep beam action are required to obtain accurate results.
- The proposed NLFEA methodology is shown to simulate the nonlinear stress/strain distributions, the sequence of nonlinear occurrences and redistribution of forces after concrete cracking and rebar yielding, and the governing failure mechanisms.
- The proposed two-stage safety assessment procedure simplifies the strength assessment process by employing the concept of factor of safety based on the load and material resistance factors. If the bridge is found overloaded in Stage 1, a more in-depth probabilistic assessment of Stage-2 is required. Stage-2 assessment is shown to predict higher reserve shear capacities than Stage-1 assessment – on average, 2.0 times for the bridges examined in this study.
- The conventional sectional methods cannot capture the nonlinear strain distribution and thus are not suitable for the analysis of deep beams. The proposed NLFEA methodology predicted 2.5 times the shear capacities on average than the sectional analyses (performed for demonstrative purposes).

- The strut-and-tie method is found to provide a strength prediction corresponding to the first yielding of the reinforcement or first crushing on the concrete, without accounting for any force redistribution. The proposed NLFEA methodology predicted 1.5 times the shear capacities on average than the strut-and-tie analyses.
- The proposed NLFEA methodology is useful when investigating the load redistribution and the sequence of nonlinear occurrences. Redistribution of the stresses with the subsequent development of nonlinear occurrences is found to be significant for the bridge bents investigated in this study.
- There is limited public funding for the rehabilitation and strengthening of the existing bridges. When applied considering required material models, NLFEA offers significant potential to correctly identify, and rank, overloaded bridges so that available funds can be directed to the most critical bridges.

## For deep foundation cap beams with helical piles,

- The traditional discrete modeling approaches has significant shortcoming in capturing the failure modes and the load capacities of the helical pile foundation systems. The influence of soil is neglected during the structural pile cap modeling while the influence of the concrete pile cap is neglected during the helical pile and soil modeling.
- As compared to the system-level model including all system components, the discrete modeling approach underestimated the load capacities by up to 33% under uplift. These large discrepancies between the discrete and system-level modeling approaches are obtained in softer soils.

- The load capacity predictions from the discrete and system-level modeling approaches converges as the soil becomes stiffer because the discrete modeling assumption of fixed boundary conditions become more realistic in stiffer soils.
- The system-level models demonstrate that the location of the helical pile termination bracket inside the concrete pile cap has a significant influence on the uplift capacity of the entire system. The bottom embedment depths resulted in premature concrete cracking at connection zone – a concern for long-term durability due. The systems incorporating bottom embedment depths failed at load capacities 25% less than those obtained from middle embedment depths. This type of failure is not considered in the traditional discrete modeling approaches.
- A well-defined 3D modeling methodology is proposed to better understand the holistic behavior of the helical pile foundation systems and more accurately quantify their load and displacement capacities, and visualize the system-level failure modes, including the premature and undesirable ones.
- The proposed methodology uses experimentally calibrated material models without requiring the use of any specific computer programs on the condition that it can capture the significant failure mechanisms demonstrated in this study. Experimental benchmark sets and how the calibration process is conducted is also defined in this study.
- The methodology uses a failure criterion based on the relative displacement of helices in the helical pile. Experimental failure reported in literatures occurred mostly when the load-displacement curve reaches a displacement equivalent to 8% of topmost helix plate diameter.

- With the increase in helical plate numbers, the pile embedment depths inside the soil and the pile cap, higher resistance is developed from shaft friction in the system-level model, ultimately increasing the uplift resistance up to 36% in the case studied.

# 6. References

The following references includes all the references used in this thesis.

AASHTO (2017) “LRFD bridge design specifications” Customary US units, 4th Edition. American Association of State Highway and Transportation Officials, Washington, DC, 566 pp.

AASHTO, 2018. “The manual for bridge evaluation”, 3rd Edition. American Association of State Highway and Transportation Officials, Washington, DC, xx pp.

ABAQUS 6.14 (2014) “Analysis user’s guide” Vol. IV, Dassault Systems, Providence, Rhode Island, 1098 pp. http://130.149.89.49:2080/v6.14/index.html

ACI Committee 318 (2019) “Building code requirements for structural concrete (ACI 318-19) and Commentary” American Concrete Institute, Farmington Hills, MI, 623 pp.

Alsaeq, H.M. (2013) “Effects of opening shape and location on the structural strength of RC deep beams with openings” In Proceedings of World Academy of Science, Engineering and Technology, 7(6): 494-499.

Akkaya, Y., Guner, S., and Vecchio, F.J. (2019) “Constitutive model for the inelastic buckling behavior of reinforcing bars” ACI Structural Journal, 116(3): 195-204. Retrieved from https://www.utoledo.edu/engineering/faculty/serhan-guner/docs/JP11_Akkaya_et_al_2019.pdf

Banerjee, P.K., and Davies, T.G. (1978) "The behavior of axially and laterally loaded single piles embedded in nonhomogeneous soils" Geotechnique, 28(3): 309–326. https://doi.org/10.1680/geot.1978.28.3.309

Barbachyn, S.M., Kurama, Y.C., and Novak, L.C. (2012) "Analytical evaluation of diagonally reinforced concrete coupling beams under lateral loads" ACI Structural Journal, 109(4): 497.

Baniya, P., Sharma, A., and Guner, S. (2018) "Evaluation of reserve shear capacities of bridge pier caps using the deep beam theory" Final Project Report, Ohio Department of Transportation, Columbus, 120 pp. Retrieved from https://www.utoledo.edu/engineering/faculty/serhan-guner/docs/R1_ODOT_STMCAP.pdf

Bunni, N.G., Scott, B., Park, R., and Priestley, M. (1982) "Stress-strain behavior of concrete confined by overlapping hoops at low and high strain rates" Journal of American Concrete Institute, 79(6): 496-498.

CSA (2014) "Design of concrete structures (CSA A23.3-14)" 6th Edition. Canadian Standards Association, Mississauga, Ontario, Canada, 290 pp.

Cervenka, V. (2008) "Global safety format for nonlinear calculation of reinforced concrete" Beton-und Stahlbetonbau, 103-S1: 37-42.

Chen, L., and Poulos, H. G. (1993) "Analysis of pile-soil interaction under lateral loading using infinite and finite elements" Computers and Geotechnics, 15(4): 189–220. https://doi.org/10.1016/0266-352X(93)90001-N

Chiluwal, S. and Guner, S. (2019) "Design recommendations for helical pile anchorages subjected to cyclic load reversals" Final Project Report, Deep Foundation Institute, Hawthorne NJ, USA, 173 pp. http://www.utoledo.edu/engineering/faculty/serhanguner/docs/R2_DFI_Helical_Pile_Anchorages.pdf

Clark, A.P. (1951) “Diagonal tension in reinforced concrete beams” Journal Proceedings, 48(10): 145-156.

Collins, M.P., and Mitchell, D. (1991) “Prestressed concrete structures” Response Publications, reprinted in 1997, Canada, 766 pp.

Das, B. M. (2017) “Shallow foundations: bearing capacity and foundation” CRC press, 400pp. https://doi.org/10.1201/9781315163871

Demir, A., Ozturk, H., and Dok, G. (2016) “3D numerical modeling of RC deep beam behavior by nonlinear finite element analysis” Disaster Science and Engineering, 2(1): 13-18.

Diab, M. A. M. (2015) “Behavior of helical pile connectors for new foundations” Ph.D. Thesis, School of Civil and Environment Engineering, University of Western Ontario, London, Ontario, Canada, 638 pp. Retrieved from https://ir.lib.uwo.ca/cgi/viewcontent.cgi?article=4736&context=etd Accessed 13/05/2019.

Dib, M., Kouloughli, S., and Hecini, M. (2019) “Numerical analysis of high capacity helical piles subjected to ground movement in weathered unstable clayey slope” Computers and Geotechnics, 110: 319–325. https://doi.org/10.1016/j.compgeo.2019.01.024

Fahmy, A., El Naggar, M. H. (2017) "Axial performance of helical tapered piles in sand" Geotechnical and Geological Engineering, 35(4): 1549–1576. https://doi.org/10.1007/s10706-017-0192-1

Gandomi, A.H., Alavi, A.H., Shadmehri, D.M., and Sahab, M.G. (2013) "An empirical model for shear capacity of RC deep beams using genetic-simulated annealing" Archives of Civil and Mechanical Engineering, 13(3): 354-369.

Gavin, K., Doherty, P., and Tolooiyan, A. (2014) "Field investigation of the axial resistance of helical piles in dense sand" Canadian Geotechnical Journal, 51(11): 1343–1354. https://doi.org/10.1139/cgj-2012-0463

George, B. E., Banerjee, S., and Gandhi, S. R. (2017) "Numerical analysis of helical piles in cohesionless soil. International" Journal of Geotechnical Engineering, 1–15. https://doi.org/10.1080/19386362.2017.1419912

Guner, S., and Carrière, J. (2016) "Analysis and strengthening of caisson foundations for tension loads" Canadian Journal of Civil Engineering, 43(5): 411–19. Retrieved from http://www.utoledo.edu/engineering/faculty/serhan-guner/docs/JP6_Guner_Carriere_2016.pdf Accessed 13/05/2019.

Guner, S., and Chiluwal, S. (2019) "Cyclic load behavior of helical pile-to-pile cap connections subjected to uplift forces" Engineering Structures (submitted) http://www.utoledo.edu/engineering/faculty/serhan-guner/docs/Guner_Chiluwal_Helical_Pile_Connections_Submitted.pdf

Guner, S., and Vecchio, F.J. (2010) "Pushover analysis of shear-critical frames: formulation" ACI Structural Journal, 107(01): 63-71. Retrieved from https://www.utoledo.edu/engineering/faculty/serhan-guner/docs/JP1_Guner_Vecchio_2010a.pdf

Howard, A.K. (1984) "The revised ASTM standard on the unified classification system" Geotechnical Testing Journal, 7(4): 216-222. 10.1520/GTJ10505J

Hu, L., and Pu, J. L. (2003) "Application of damage model for soil–structure interface" Computers and Geotechnics, 30(2): 165–183. https://doi.org/10.1016/S0266-352X(02)00059-9

Hwang, S.J., and Lee, H.J. (2002) "Strength prediction for discontinuity regions by softened strut-and-tie model" Journal of Structural Engineering, 128(12): 1519-1526.

Kani, G. (1967) "How safe are our large reinforced concrete beams?" Journal Proceedings, 64(3): 128-141.

Kim, H.S., Lee, M.S., and Shin, Y.S. (2011) "Structural behaviors of deep RC beams under combined axial and bending force" Procedia Engineering, 14: 2212-18.

Kwon, O., Lee, J., Kim, G., Kim, I., and Lee, J. (2019) "Investigation of pullout load capacity for helical anchors subjected to inclined loading conditions using coupled Eulerian-Lagrangian analyses" Computers and Geotechnics, 111: 66–75. https://doi.org/10.1016/j.compgeo.2019.03.007

Lanyi-Bennett, S. A., and Deng, L. (2018) "Axial load testing of helical pile groups in a glaciolacustrine clay" Canadian Geotechnical Journal, 56(2): 187–197. https://www.nrcresearchpress.com/doi/pdfplus/10.1139/cgj-2017-0425

Lee, J., and Fenves, G. L. (1998) “Plastic-damage model for cyclic loading of concrete structures” Journal of Engineering Mechanics, 124(8): 892–900. https://doi.org/10.1061/(ASCE)0733-9399(1998)124:8(892)

Livneh, B., El Naggar, M. H. (2008) “Axial testing and numerical modeling of square shaft helical piles under compressive and tensile loading” Canadian Geotechnical Journal, 45(8): 1142–1155. https://doi.org/10.1139/T08-044

Lubliner, J., Oliver, J., Oller, S., and Oñate, E. (1989) “A plastic-damage model for concrete” International Journal of Solids and Structures, 25(3): 299–326. https://doi.org/10.1016/0020-7683(89)90050-4

Lutenegger, A. J. (2015) “Quick design guide for screw-piles and helical anchors in soils” International Society for Helical Foundations, 13 pp.

Mohajerani, A., Bosnjak, D., and Bromwich, D. (2016) “Analysis and design methods of screw piles: a review” Soils and Foundations, 56(1): 115–128. https://doi.org/10.1016/j.sandf.2016.01.009

NAVFAC. (2019) “Table of Ultimate Friction Factors for Dissimilar Materials” Retrieved May 13, 2019, from <https://www.scribd.com/document/386017978/Table-of-Ultimate-Friction-Factors-for-Dissimilar-Materials>

Niranjan, B.R., and Patil, S.S. (2012) “Analysis of R.C deep beam by finite element method” International Journal of Modern Engineering Research (IJMER), 2(6): 4664-4667.

Oh, J.K., and Shin, S.W. (2001) “Shear strength of reinforced high-strength concrete deep beams” Structural Journal, 98(2): 164-173.

Özcan, D.M., Bayraktar, A., Şahin, A., Haktanir, T., and Türker, T. (2009) "Experimental and finite element analysis on the steel fiber-reinforced concrete (SFRC) beams ultimate behavior" Construction and Building Materials, 23(2): 1064-1077.

Pan, Z., Guner, S., and Vecchio, F.J. (2017) "Modeling of interior beam-column joints for nonlinear analysis of reinforced concrete frames" Engineering Structures, 142: 182-191.

Popovics, S. (1973) "A numerical approach to the complete stress-strain curve of concrete" Cement and Concrete Research, 3(5): 583-599.

Perko, H. A. (2009) "Helical piles: A practical guide to design and installation" New Jersey: John Wiley & Sons, Inc, 512 pp. https://doi.org/10.1002/9780470549063.ch12

Quintero-Febres, C.G., Parra-Montesinos, G., and Wight, J.K. (2006) "Strength of struts in deep concrete members designed using strut-and-tie method" ACI Structural Journal, 103(4): 577.

Randolph, M. F. (1977) "A theoretical study of the performance of the piles" Ph.D. Thesis, Department of Engineering, University of Cambridge, 260 pp. Retrieved from https://www.repository.cam.ac.uk/handle/1810/250739 Accessed 13/05/2019.

Rawat, S. and Gupta, A. K. (2017) "Numerical modelling of pullout of helical soil nail" Journal of Rock Mechanics and Geotechnical Engineering, 9(4): 648–658. https://doi.org/10.1016/j.jrmge.2017.01.007

Rogowsky, D.M., and MacGregor, J.G. (1986) "Design of reinforced concrete deep beams" Concrete International, 8(8): 49-58.

Sakr, M. (2013) "Comparison between high strain dynamic and static load tests of helical piles in cohesive soils" Soil Dynamics and Earthquake Engineering, 54: 20–30. https://doi.org/10.1016/j.soildyn.2013.07.010

Sakr, M. (2011) "Installation and performance characteristics of high capacity helical piles in cohesionless soils" DFI Journal-The Journal of the Deep Foundations Institute, 5(1): 39–57. https://doi.org/10.1179/dfi.2011.004

Salgado, R.A., and Guner, S. (2018a) "A comparative study on nonlinear models for performance-based earthquake engineering" Engineering Structures, 172: 382-391. Retrieved from https://www.utoledo.edu/engineering/faculty/serhan-guner/docs/JP10_Salgado_Guner_2018.pdf

Salgado, R.A., and Guner, S. (2018b) "Numerical analysis methodology for deep cap beams retrofitted with fiber reinforced polymers" Advances in Concrete Bridges; Design, construction, evaluation, and rehabilitation, American Concrete Institute, SP 331-1: 1-10. Retrieved from https://www.utoledo.edu/engineering/faculty/serhan-guner/docs/JP14_Salgado_Guner_2019.pdf

Salhi, L., Nait-Rabah, O., Deyrat, C., and Roos, C. (2013) "Numerical modeling of single helical pile behavior under compressive loading in sand" EJGE, 18: 4319–4338. http://www.ejge.com/2013/Ppr2013.395mlr.pdf

Schlaich, J., Shafer, K., and Jennewein, M. (1987) "Toward a consistent design of structural concrete" PCI Journal, 32(3): 171-179.

Schlaich, J., and Shafer, K. (1991) "Design and detailing of structural concrete using strut-and-tie models" Structural Engineer, 69(6): 113-125.

Scott, R.M., Mander, J.B., and Bracci, J.M. (2012) "Compatibility strut-and-tie modeling: Part I-Formulation" ACI Structural Journal, 109(5): 635.

Senturk, A.E., and Higgins, C. (2010a) "Evaluation of RCDG bridge bent caps with 1950's Vintage Details - Analytical Methods" ACI Structural Journal, 107(5): 544-553.

Senturk, A.E., and Higgins, C. (2010b) "Evaluation of RCDG bridge bent caps with 1950's Vintage Details – Laboratory Tests" ACI Structural Journal, 107(5): 534-543.

Senturk, A.E. (2008) "Experimental and analytical evaluation of conventionally reinforced deck-girder bridge bent caps with vintage details" PhD Dissertation, Oregon State University, 351 pp.

Sun, D. A., Yao, Y. P., and Matsuoka, H. (2006) "Modification of critical state models by Mohr–Coulomb criterion" Mechanics Research Communications, 33(2): 217–232. https://doi.org/10.1016/j.mechrescom.2005.05.006

Tan, K.H., Kong, F.K., Teng, S., and Weng, L.W. (1997) "Effect of web reinforcement on high-strength concrete deep beams" Structural Journal, 94(5): 572-582.

Tan, S. A., Ooi, P. H., Park, T. S., and Cheang, W. L. (2008) "Rapid pullout test of soil nail" Journal of Geotechnical and Environmental Engineering, 134(9): 1327–1338. https://doi.org/10.1061/(ASCE)1090-0241(2008)134:9(1327)

Vecchio, F. J., and Shim, W. (2004) " Experimental and analytical reexamination of classic concrete beam tests" Journal of Structural Engineering, 130(3): 460–469. https://doi.org/10.1061/(ASCE)0733-9445(2004)130:3(460);

Vecchio, F.J., and Collins, M.P. (1986) "The modified compression-field theory for reinforced concrete elements subjected to shear" ACI Journal, 83(2): 219-231.

Vecchio, F.J. (2000) “Disturbed stress field model for reinforced concrete: formulation” Journal of Structural Engineering, 126(9): 1070-1077.

Wong, P.S., Vecchio, F.J., and Trommels, H. (2013) “VecTor2 and FormWorks user’s manual” Technical Report, Department of Civil Engineering, University of Toronto, 347 pp. Retrieved from http://www.vectoranalysisgroup.com/user_manuals/manual1.pdf

Young, J.J.M. (2012) “Uplift capacity and displacement of helical anchors in cohesive soil” MS Thesis, School of Civil and Construction Engineering, Oregon State University, 156 pp. Retrieved from https://ir.library.oregonstate.edu/downloads/j6731765j Accessed 13/05/2019.

Zhou, W. H., Yin, J. H., and Hong, C. Y. (2011) “Finite element modelling of pullout testing on a soil nail in a pullout box under different overburden and grouting pressures” Canadian Geotechnical Journal, 48(4): 557–567. https://doi.org/10.1139/t10-086.